UiA University of Agder

Master

Analysis of Spectral Irradiance Variations and Their Impact on the Performance of Different Photovoltaic Modules

ADRIAN BJØRGE ULVEN

SUPERVISOR
ANNE GERD IMENES

University of Agder, 2023
Faculty of Engineering and Science
Department of Engineering and Sciences

Obligatorisk gruppeerklæring

Den enkelte student er selv ansvarlig for å sette seg inn i hva som er lovlige hjelpemidler, retningslinjer for bruk av disse og regler om kildebruk. Erklæringen skal bevisstgjøre studentene på deres ansvar og hvilke konsekvenser fusk kan medføre. Manglende erklæring fritar ikke studentene fra sitt ansvar.

1.	Vi erklærer herved at vår besvarelse er vårt eget arbeid, og at vi ikke har brukt andre kilder eller har mottatt annen hjelp enn det som er nevnt i besvarelsen.	Ja
2.	**Vi erklærer videre at denne besvarelsen:** • Ikke har vært brukt til annen eksamen ved annen avdeling/universitet/høgskole innenlands eller utenlands. • Ikke refererer til andres arbeid uten at det er oppgitt. • Ikke refererer til eget tidligere arbeid uten at det er oppgitt. • Har alle referansene oppgitt i litteraturlisten. • Ikke er en kopi, duplikat eller avskrift av andres arbeid eller besvarelse.	Ja
3.	Vi er kjent med at brudd på ovennevnte er å betrakte som fusk og kan medføre annullering av eksamen og utestengelse fra universiteter og høgskoler i Norge, jf. Universitets- og høgskoleloven §§4-7 og 4-8 og Forskrift om eksamen §§ 31.	Ja
4.	Vi er kjent med at alle innleverte oppgaver kan bli plagiatkontrollert.	Ja
5.	Vi er kjent med at Universitetet i Agder vil behandle alle saker hvor det forligger mistanke om fusk etter høgskolens retningslinjer for behandling av saker om fusk.	Ja
6.	Vi har satt oss inn i regler og retningslinjer i bruk av kilder og referanser på biblioteket sine nettsider.	Ja
7.	Vi har i flertall blitt enige om at innsatsen innad i gruppen er merkbart forskjellig og ønsker dermed å vurderes individuelt. Ordinært vurderes alle deltakere i prosjektet samlet.	Ja

Publiseringsavtale

Fullmakt til elektronisk publisering av oppgaven Forfatter(ne) har opphavsrett til oppgaven. Det betyr blant annet enerett til å gjøre verket tilgjengelig for allmennheten (Åndsverkloven. §2).
Oppgaver som er unntatt offentlighet eller taushetsbelagt/konfidensiell vil ikke bli publisert.

Vi gir herved Universitetet i Agder en vederlagsfri rett til å gjøre oppgaven tilgjengelig for elektronisk publisering:	Ja
Er oppgaven båndlagt (konfidensiell)?	Nei
Er oppgaven unntatt offentlighet?	Nei

Acknowledgements

This thesis is culmination of a long education at Univeristy of Agder and will mark as the completion of my masters program within Renewable energy.

First I would like to give my thanks to my supervisor Prof. Anne Gerd Imenes for her excellent guidance and dedication throughout this semester. I am very grateful for her willingness to go the extra mile to help me out. I also want to thank Prof. Joao Leal for his amazing willingness to help with python coding. Finally, I would like to thank my friends for making my time studying Renewable Energy at the University of Agder unforgettable.

Abstract

I denne avhandlingen har to år med global horisontal spektral innstrålings og global vinklet spektral innstrålings data har blitt analysert for å se hvordan spektral distribusjoen varierer over disse to årende. I tillegg skal det prøves å estimere energi utbyttet fra fire forkjellige PV moduler, ved bruk av de to årene med global horisontal og vinklet spektral innstråling. Disse modulene er en c-Si modul, en a-Si modul, en CdTe modul og en CIGS modul. I utgangspunktet skulle oppgaven gå ut på å teste et håndholdt spektrometer og bli sammenlignet med et stasjonært spektrometer. Grunnet et defekt kalibrerings instrument kunne ikke dette bli undersøkt videre og hovedfokuest ble satt på spektral dataene. Et gjennomsnittlig spektral distribusjonen for hver måned ble laget untatt for månedene som manglet i data settet. Energi utbytte for de fire PV modulene ble estimert gjennom et python-skript. Energi utbyttet som ble regnet ut viste seg å være ikke riktige grunnet en feil i data prosseseringen i metode delen. Målingene til CIGS PV modulen spesifikt virket også til å være noe galt med grunnet dens høye ytelse i forhold til de andre modulene.

This thesis analyzes two years of global horizontal spectral irradiance and global tilted spectral irradiance data to see how the spectral distribution varies over these years. In addition, an attempt will be made to estimate the energy yield from four different PV modules using two years of global horizontal and angled spectral radiation. These modules are a c-Si module, an a-Si module, a CdTe module, and a CIGS module. Initially, the task was to test a hand-held spectrometer and be compared with a stationary spectrometer. Due to a defective calibration instrument, this could not be investigated further, and the main focus of the thesis was moved to the spectral data. An average spectral distribution for each month was created except for the months that were missing from the data set. The energy yield for the four PV modules was estimated through a Python script. The energy yield that was calculated turned out to be incorrect due to an error in the data processing in the method section. The measurements of the CIGS PV modules were also off due to their high performance compared to the other modules.

Contents

List of Figures

List of Tables

Chapter 1

Introduction

The world is moving towards the green shift, and the growing demand for renewable energy sources has made solar energy one of the fastest-growing alternatives to fossil fuel. It has made significant strides over the last few decades. Photovoltaic (PV) technology produces energy through sunlight by absorbing the photons radiated from the sun. PV module's performance depends on various factors, such as irradiance levels, module temperature, and solar spectrum distribution. Understanding these factors is important for optimizing the efficiency of PV systems.

This thesis aims to analyze two years of global horizontal spectral irradiance (GHI) and global tilted spectral irradiance (GTI) data to see how the spectral distribution changes based on the incidence angle for each month and how spectral characteristics influence PV module performance. Furthermore, the study will also estimate the energy output for different PV modules such as crystalline silicon (c-Si), amorphous silicon (a-Si), copper indium gallium selenide (CdTe), and cadmium telluride (CiGS) for two years. Initially, as part of this thesis, a high-speed miniature fiber optic spectrometer HR2000+ was to be tested and compared with a stationary broadband Spectrafy instrument. The idea was to measure the incident sunlight at multiple different tilt angles from 90 to 0 degrees and with different orientations to see how the different angles affected spectral distribution and potentially the energy yield of solar devices. However, a defect calibration tool meant this part could not be further investigated. Hence, the focus of this thesis is on the analysis of two years of spectral irradiance distribution collected in two different planes. The data material for spectral irradiance measurements is scarce, particularly for the Nordic regions, so investigating this data could be interesting.

1.1 Research question

This thesis aims to analyze two years of spectral data for global irradiance measurement in the horizontal plane and in the tilt plane of 45° (optimum tilt for the location of Grimstad, Norway), i.e., GHI and GTI to investigate how global horizontal and global tilted spectral irradiance changes by month, and how do these variations impact the energy output of different photovoltaic modules?
The objectives of this research are as follows:

• To analyze and compare the GHI and GTI data that has been collected for two years to determine any significant trends or patterns in the spectral distribution.

• To create spectral distribution graphs for each month to show how irradiance changes for two years for both tilted and horizontal planes.

• To estimate the energy output of 4 different PV module types using spectral data while accounting for factors such as temperature.

• To test a high-speed miniature fiber optic spectrometer and compare the measurements from a stationary broadband Spectrafy instrument.

1.2 Thesis structure

This thesis consists of five chapters. The first chapter gives an introduction to the thesis with the research question. The second chapter will be a theoretical background explaining concepts and equations used in the thesis. The third part will go through the methodology of how the investigation was undertaken. The fourth chapter will present and discuss the calculated data and results. Finally, the last chapter will give a conclusion to the thesis.

Chapter 2

Theoretical background

This section will go through theory, concepts and equation used in this thesis, and at the end of the chapter a literature review will be presented.

2.1 Solar radiation

The sun's energy originates from a nuclear reaction in the core of the sun, it is then transmitted to the surface of the sun and radiated into space. This energy is a form of electromagnetic radiation that consists of photons where the photon energy is characterised by its wavelength. The energy travels through space and is radiated on the surface of the earth. This radiation is defined as 1361W/m^2 (the solar constant) perpendicular to the sun's rays. Due to the shape and declination of the earth, the radiation hits the surface at different angles. This causes the light to travel a longer distance through the atmosphere near the poles (in the morning/evening at low solar elevation), making the light more scattered and diffuse. [1]

Peak sun hours is the average daily solar insolation in units of kWh/m2 per day. Peak solar radiation is 1kW/m2 and it refers to the solar isolation a specific location would receive as if the sun were shining at its maximum for a certain number of hours. Since the number of peak sun hours is identical to the average daily solar isolation, means that if a location receives 7 kWh/m2 per day can be then said to have received 7 hours of sun per day at 1 kW/m2[2]

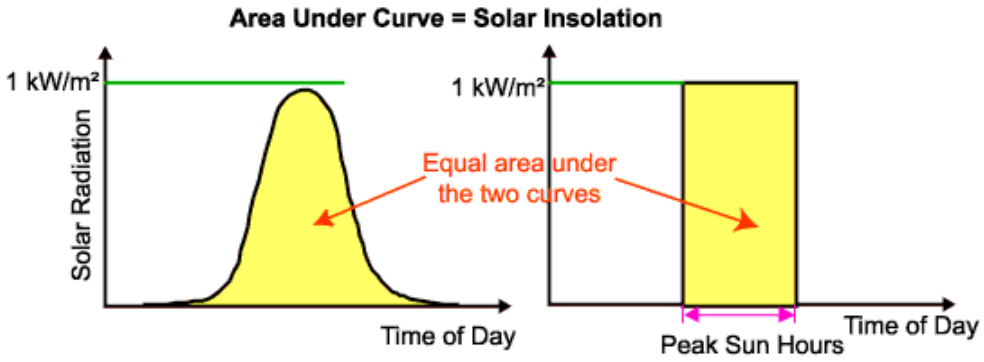

Figure 2.1: Illustration of peak sun hours. Source: www.pveducation.org **empty citation**

The irradiance the PV modules are exposed to can be divided up into different components. Diffuse radiation is light that is scattered in the atmosphere, reflected radiation is light that is reflected by various surfaces and direct radiation is light that is neither scattered or reflected. These three components make up global radiation and can be seen in 2.2. Global horizontal irradiance (GHI) is the total of direct and indirect sunlight received on a flat surface and it serves as a standard measure for comparing different climate zones. Global

tilted irradiance (GTI) is the total sunlight received on a surface that has a specific tilt and orientation. It is the sum of the scattered radiation, direct and reflected [3]. Figure 2.2 is an illustration of the different irradiance components.

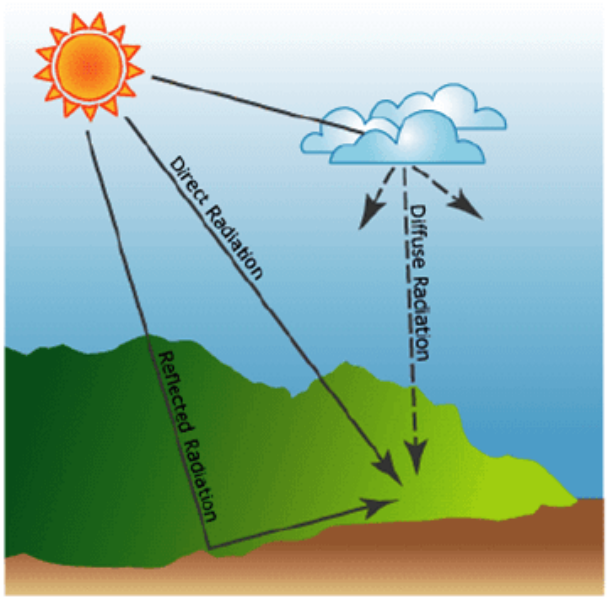

Figure 2.2: The difference between the various components of radiation PV modules are exposed to. Source: www.yellowhaze.com [4]

2.1.1 Electromagnetic spectrum

Electromagnetic radiation travels through space in a wave-like pattern. The wavelength of these waves determine the amount of energy it carries, shorter wavelength means more energy and longer wavelength means lower energy. Wavelength, energy and frequency are ways to express the electromagnetic spectrum. Figure 2.3 shows an illustration of the electromagnetic spectrum and how it is divided up.

$$\lambda = \frac{c}{f} \tag{2.1}$$

where λ is the wavelength, c is the speed of light at 299,792,458 m/s and f is the frequency

$$E = h \cdot f \tag{2.2}$$

where E is energy and h is Planck's constant (6.626 x 10-34 Js). [5]

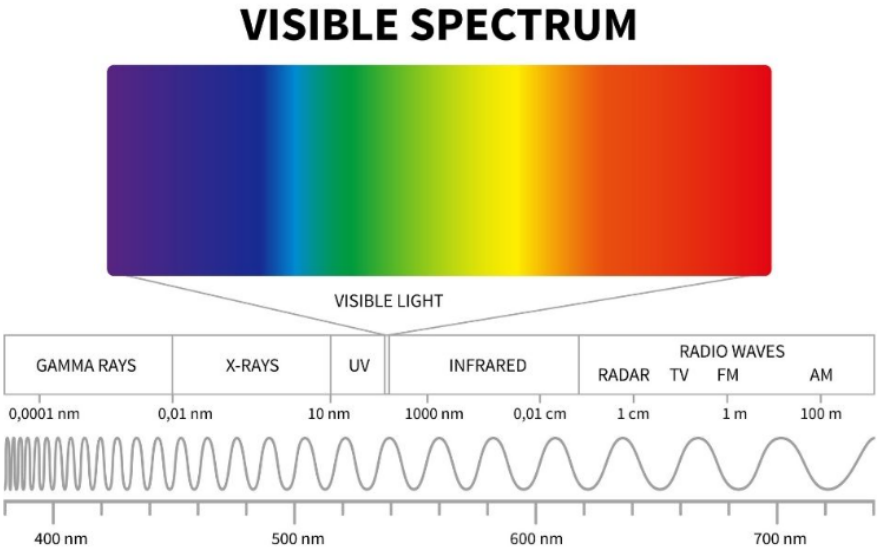

Figure 2.3: The electromagnetic spectrum: Source: NASA [5]

2.2 Spectral irradiance

Spectral irradiance as a function of photon wavelength is a common way of characterizing a light source. It is measured in $\mathrm{Wm}^{-2}\ \mu\mathrm{m}^{-1}$, where Wm^{-2} is the power density at the wavelength $\lambda(\mu\mathrm{m})$. When analysing solar cells it is often useful to calculate the photon flux, since the spectral irradiance can be determined from the photon flux. Photon flux can be used to calculate the spectral irradiance by converting the photon flux at a specific wavelength to $\mathrm{W/m}^2$. This result is then divided by the wavelength in micrometers to obtain the spectral irradiance. [6]

2.2.1 Air mass

Air mass (AM) is the path light has to travel through the atmosphere. It is calculated based on the sun's zenith angle, Where AM1 is directly above and AM2 is twice the length of AM1. As long as the sun is not very near the horizon, air mass can be calculated through the equation:

$$AM = \frac{1}{cos\theta} \tag{2.3}$$

where θ is the zenith angle. [7]

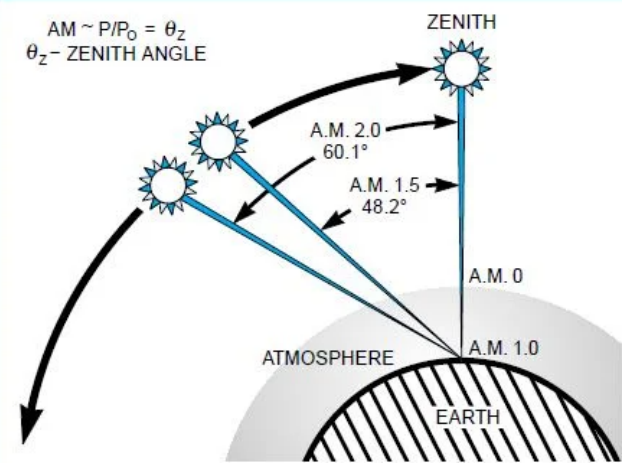

Figure 2.4: The path length, in units of Air Mass, changes with the zenith angle. Source: www.azom.com [8]

2.3 Standard test conditions

The performance of PV modules varies a lot depending on location and environmental conditions, which means it is difficult to accurately estimate the performance of PV modules in the field. In order to compare PV modules, a set of conditions known as the standard test conditions have been made for manufacturers as way to define the electrical performance of their photovoltaic modules. The STC for PV modules is defined as being 1000 W/m^2 irradiance, the standard temperature of the cell is at 25°C and a sea level air mass of 1.5 [9].

2.4 Harnessing sunlight using photovoltaic technology

A photovoltaic (PV) cell is simply put a semiconductor device that converts light from the sun into DC electricity and these cells make up a PV module. Most cells are generally made of highly purified silicon, although there are many different types of semiconductors, crystallized silicon is the most widely used. A typical c-Si cell has two layers, the top layer, known as N-type, has been doped with phosphorus. The bottom layer, known as P-type, has been doped with boron. When a photons hits the cell it knocks an electron of a silicon atom, this electron moves to the top layer. By connecting the top and bottom layer with a metal wire will cause the electrons to move from the the top layer via an external circuit to the bottom layer, thus creating an electrical current. [10]

A PV module is made up of many PV cells, when they are wired in parallel they increase current and in series to produce higher voltage. A module is encapsulated in a transparent material, usually EVA, and with a tempered glass on the surface. The edges are sealed to protect the cells in the module. To hold everything together a aluminum frame is often used. The back side of the module there are wires and electrical connections. There are various types of PV modules and the structure of the module often differ for different modules. Examples of different types are crystalline silicon (poly-Si and mono-Si are both c-Si), amorphous silicon (a-Si), copper indium gallium selenide (CdTe) and cadmium telluride (CiGS) [11]. Figure 2.5 shows a schematic of a PV module.

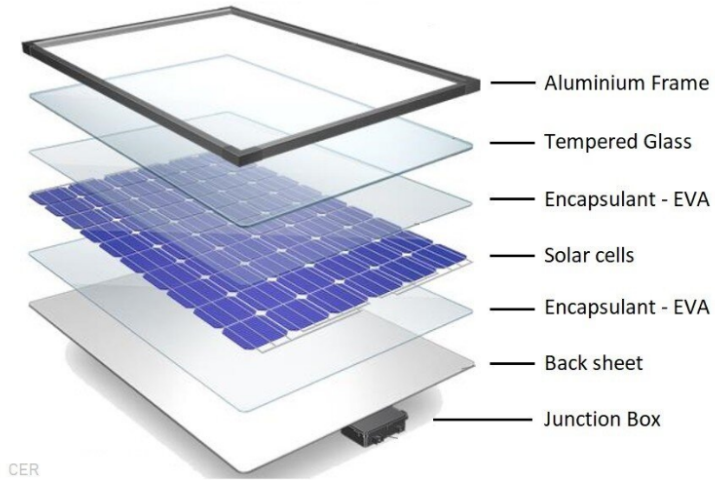

Figure 2.5: A schematic of a typical PV module. Source: www.cleanenergyreviews.info [12]

mono-Si is the most efficient, however, it is the most expensive due to the higher performance and manufacturing process that is required for these types [13]. In 2011 crystalline silicon PV cells make up 85% of the PV world marked. Their efficiency under STC ranges form 18& - 22% [14]

a-Si is a non-crystalline type of the silicon semiconductor. According to www.sinovoltaics.com [15] it has high absorption capabilities, which allows solar cells to be produced with significantly thinner layers, which can typically be around 100 times thinner than crystalline silicon, this saves on material costs and offsets its relatively low maximum efficiency of around 13%. Although amorphous silicon solar cells do not perform as well as their c-Si counterparts, they can be deposited at much lower temperatures and onto different structures, including not just glass but also plastic. a-Si cells was mostly used in low-power electronics items such as calculators and watches due to their simpler and more cost-effective production. Now however, due to advancements in production techniques have expanded the applications of a-Si modules, such as in building-integrated photovoltaics (BIPV) [15].

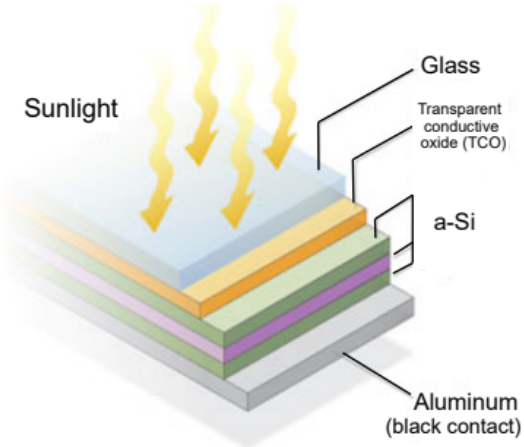

Figure 2.6: A schematic of a typical a-Si PV module. Source: www.solarreviews.com [16]

According to www.energy.gov [17] the CdTe solar cells currently makes up 5% of the world marked, this makes it the second most common in the world. The benefits of CdTe PV modules are its inexpensive manufacturing and quick production, additionally, cadmium telluride is a direct-bandgap material with bandgap energy that allows it to be tuned from 1.4 eV to 1.5 eV, which is nearly optimal for energy production. [17].

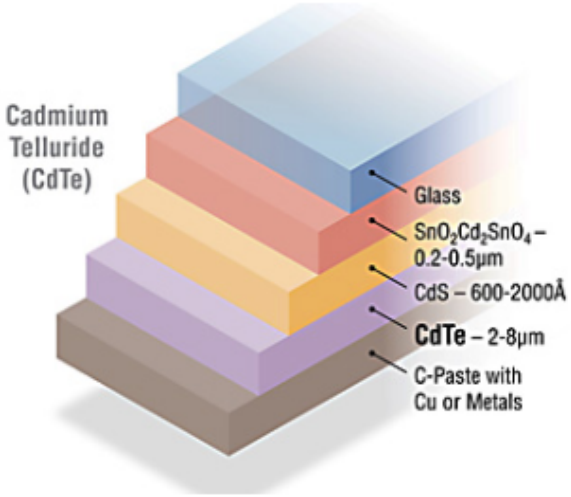

Figure 2.7: A schematic of a typical CdTe PV device. Source: www.nrel.gov [18]

CIGS solar panels are another type of thin-film solar panel that have shown real-world efficiencies in the range of 10-12 percent. These modules uses less harmful materials than some other types.Figure 2.8 shows an schematic of a CIGS substrate thin-film PV device. The layers are applied onto a substrate made of metal, plastic or glass. The top layer, known as TOC, allows sunlight to enter, which results in the generation of electrical current and voltage within the lower layers.

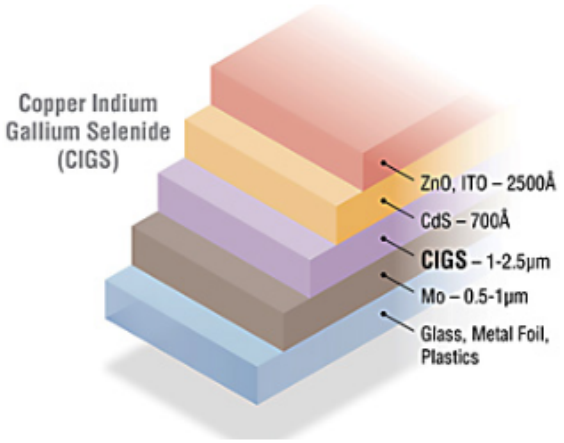

Figure 2.8: An illustration of a CIGS device. Source: www.nrel.gov [19]

2.5 Average photon energy

Average photon energy is often used as a parameter to characterize spectral irradiance in literature. APE is defined as the mean energy value of all photons from a given solar spectrum distribution [20]. The APE value highly depends on the wavelength range it is integrated over. The APE value for the AM 1.5G reference spectrum is 1.88 eV if the wavelength range is from 350 - 1050 mn, this value lowers down to 1.59 eV if the range is increased to 350 - 1700 mn [21]. Overhead clouds and humid weather can affect the APE value as clouds can absorb light with long wavelengths, which will cause the APE value to increase. A high APE value is often referred to as "blue rich", while a low APE value is referred to as "red rich"[22]. APE can be calculated using this formula:

$$APE = \frac{1}{q}\left(\frac{\int_a^b E_\lambda d\lambda}{\int_a^b \phi_\lambda d\lambda}\right) \tag{2.4}$$

where E_λ is the spectral irradiance at wavelength (λ), q is the elementary charge (1.602×10^{19} coulombs) and ϕ_λ is the photon flux density, a and b are the integration limits.

Photon flux density (Photons/$m^{-2}\cdot$ $s^{-1}\cdot$ nm^{-1}) can be calculated using this formula:

$$\phi_\lambda = \frac{E_\lambda}{\frac{hc}{\lambda}} \tag{2.5}$$

where h is the Planck's constant (6.626×10^{-34} Js), c is the speed of light (3×10^8 m/s) in a vacuum and λ is the wavelength.

2.6 Quantum efficiency

Quantum efficiency is defined as the amount of current a solar cell can produce when exposed to irradiance of a specific spectrum. By integrating the cell's spectral quantum efficiency over the solar electromagnetic spectrum, the current produced by the cell can be estimated under exposure to sunlight. When comparing the actual energy output of the solar cell to its maximum potential energy output, it is possible to get the overall energy conversion efficiency value. Internal quantum efficiency (IQE) is the ratio between the number of charge carriers captured by the solar cell compared to the number of photons of a given energy that enter into th soalr cell. On the other hand, external quantum efficiency (EQE) is the ratio of charge carriers collected by the solar cell relative to the number of photons having a given energy value that is shining from the outside, and includes reflection loss.[23]

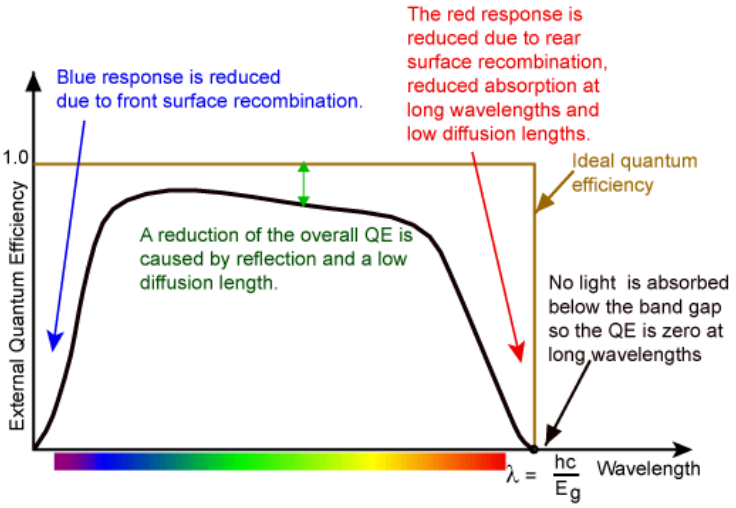

Figure 2.9: The quantum efficiency of a silicon solar cell. Source: www.pveducation.org [24]

2.7 Open-circuit voltage

The open-circuit voltage (V_{oc}) is the highest voltage available from a solar cell, when there is no current flowing. This voltage corresponds with the forward bias applied to the solar cell junction, which results from the interaction between the light-generated current and the solar cell itself. [25]

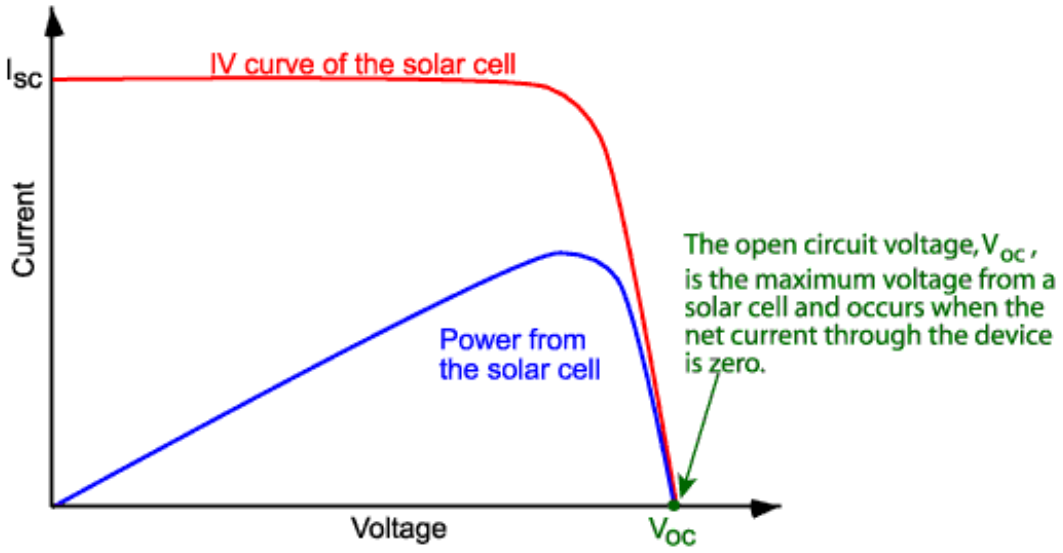

Figure 2.10: The IV curve of a solar cell. Source: www.pveducation.org [25]

V_{oc} can be calculated by this equation:

$$Voc = \frac{nkT}{q} ln(\frac{I_L}{I_0} + 1) \tag{2.6}$$

where n is the ideality factor, k is the Boltzmann constant, T is the temperature in kelvin, I_L is the light generated current and I_0 is the dark saturation current. [25]

2.8 Short-circuit current

The short-circuit current (I_{sc}) is the current flowing through a solar cell when the voltage is zero, meaning the solar cell is in a short-circuited state. The current comes from the light-generated particles that create electricity in the solar cell. In an ideal situation, where there is no energy loss, the short-circuit current is the same as the current produced by the light. The I_{sc} is affected by various factors, such as: The area of the solar cell, the number of photons, the spectrum of the incident light and the optical properties. Calculating I_{sc} can be done by this equation:

$$Isc = (qG(L_n + L_p))A \tag{2.7}$$

where q is the elementary electron charge, G is the generation rate L_n and L_p are the electron and hole diffusion lengths respectively and A is the area of the cell. [26]

2.9 Fill factor

Like previously mentioned, both open-circuit voltage and short-circuit current are the maximum voltage and current from a solar cell. However, at these points there is no power output from the solar cell. The parameter known as "fill factor" works in conjunction with I_{sc} and V_{oc} to determine the maximum power of a solar cell [27]. It can be calculated with the following equation:

$$FF = \frac{V_{MP} * I_{MP}}{V_{OC} * I_{SC}} \tag{2.8}$$

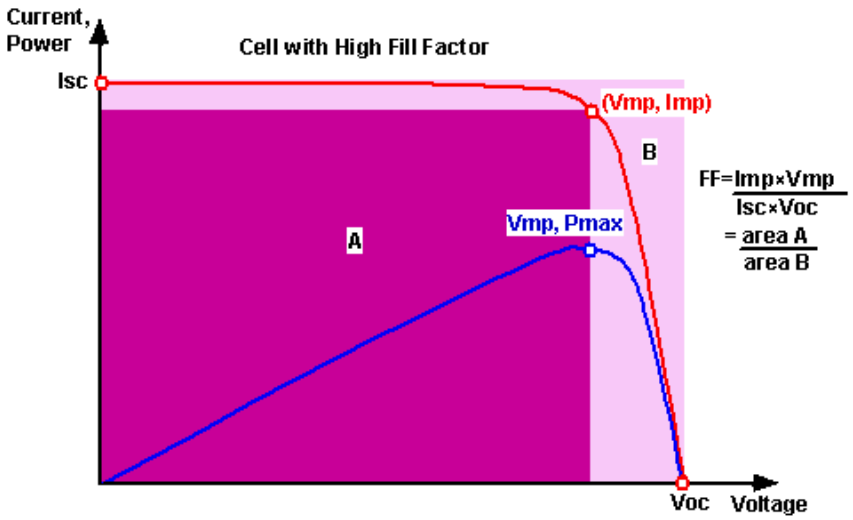

Figure 2.11: Illustration showing fill factor. Source: www.pveducation.org [27]

By using the three previously mentioned parameters, P_{max} can be calculated, which is the point where the voltage and current creates the highest power. [28]

$$Pmax = I_{SC} * V_{OC} * FF \tag{2.9}$$

2.10 Effect of temperature

Semiconductors are sensitive to temperature, this is also the case for solar cells. When the temperature rises, the semiconductor's bandgap decreases, affecting most of its material properties. This reduction in the bandgap can be seen as an increase in the electron energy within the material, requiring less energy to break the bond. The effects of temperature is complex and it differs depending on the solar cell technology. Figure 2.12 shows the impact temperature has on open-circuit voltage. [29]

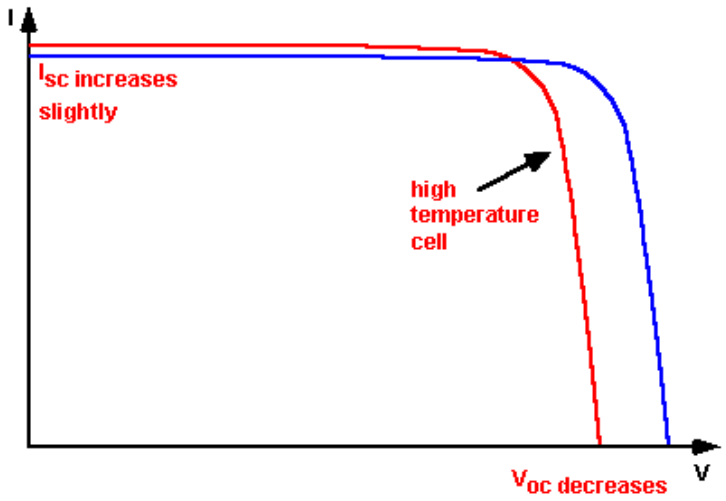

Figure 2.12: The effects of temperature on a IV curve of a solar cell. Source: www.pveducation.org [29]

Short circuit current (I_{sc}) is also affected by temperature although not to the same extent as V_{oc}. The I_{sc} shows a slight increase as the temperature rise. This happens because the bandgap energy (E_G) decreases, allowing a greater number of photons to get sufficient energy

to generate electron-hole pairs. This however, is a relatively minor difference and its impact is typically minimal, with around 0.06% per °C. [29]

2.11 Nominal operating cell temperature

PV modules are normally rated after the STC, however, the PV modules are not exposed to the same conditions when operating in the field. They can operate at both higher and lower temperatures, which will affect the power output of the module. The Nominal Operating Cell Temperature (NOCT) refers to the temperature that cells within a module achieve when they are open-circuited, given the conditions that irradiance on the cell is 800W/m^2, air temperature is 20°C, wind speed is 1m/s and the mounting is open back side. To calculate the cell temperature using NOCT only gives an approximate temperature as there are various factors that can affect its accuracy. [30]

$$T_{cell} = T_{air} + (\frac{NOCT - 20}{80}) * S \tag{2.10}$$

Where T_{air} is the ambient temperature, $NOCT$ is the cell temperature at NOCT and S is the total irradiance the cell is exposed to in W/m^2 [30]. To calculate the new P_{max} with temperature accounted for can be done through this equation:

$$PmaxT = Pmax - Pmax * (P_{coeff}/100) * (25 - T_{cell}) \tag{2.11}$$

where P_{maxT} is the new P_{max} with temperature accounted for, P_{coeff} is the temperature coefficient of P_{max} and T_{cell} is the temperature of the cell.

When calculating the cell temperature, there are other ways of doing this than through the NOCT method. One such example is the so-called Sandia Photovoltaic Array Performance Model (SAM), which is based on an article by King (2004) [31]

$$T_m = E \times e^{(a+b\times WS)} + T_a \tag{2.12}$$

$$T_C = T_m + \frac{E}{E_0}\Delta T \tag{2.13}$$

where Tm is the module temperature, E is the plane-of-array irradiance (W/m^2), a and b are configurations based on both the module construction and its mounting, WS is the wind speed and Ta is the ambient air temperature.

2.12 Resistance within the PV system

Temperature is not the only factor affecting power production in a PV module, internal resistance within the PV module can also affect it. Significant power loss can be attributed to the presence of a shunt resistance, although this is usually due to manufacturing defects and not poor solar cell design itself. A low shunt resistance causes power losses in the cells due to it giving the light-generated current an alternative path. This causes a reduced amount of current flowing through the cell junction and in turn lowering the cell's voltage. This effect is especially severe during low light levels, as there is less light-generated current in those situations. [32]

Series resistance is also affecting PV modules and it arises from three sources. The first one is the current's flow through the solar cell's emitter and base. The second is contact resistance between the metal contact and silicon. The third is the resistance of the top and rear metal contacts. Series resistance mainly causes a reduction in fill factor, although at

exceedingly high values it can also reduce the short circuit current. Figure 2.13 shows how shunt and series resistance can affect an IV curve.[33]

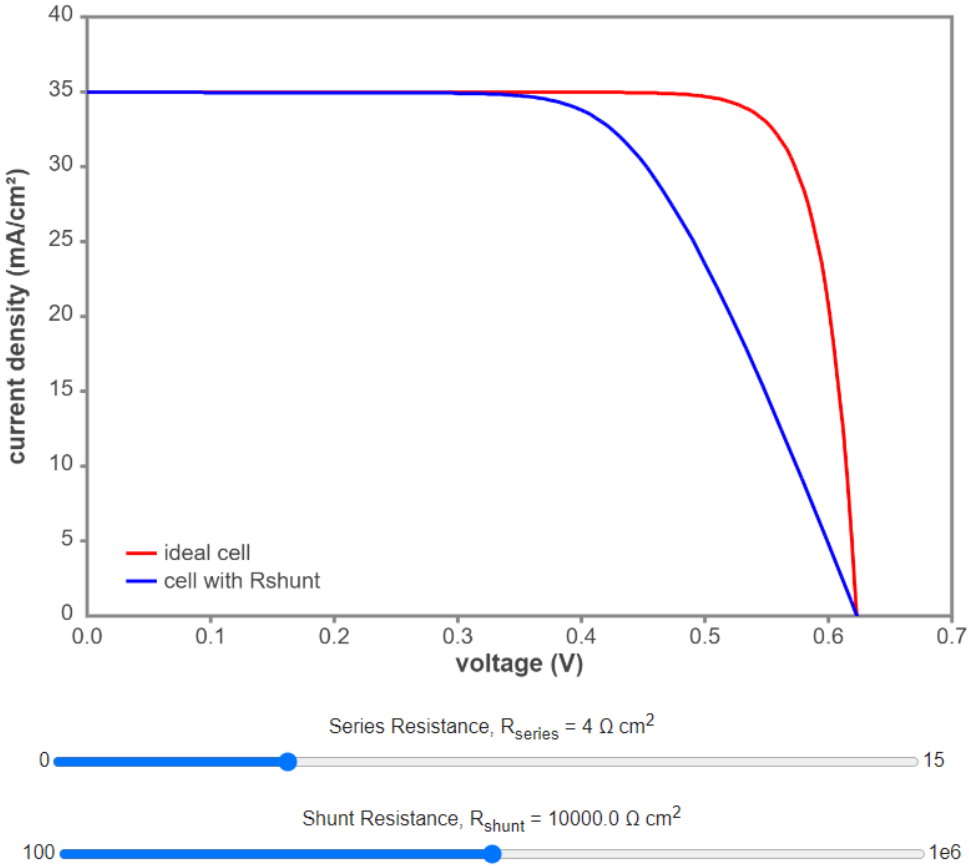

Figure 2.13: The effect of shunt and series resistance on a IV curve. Source: www.pveducation.org [34]

2.13 Literature review

Erin E. Looney et al. (2020) [35] propose a method of classification of spectral irradiance curve based on an iterative use of the k-means clustering algorithm, they have called this method RISE (Representative Identification of Spectra and the Environment). By defining a set of 18 spectra using RISE they can reproduce the impact on energy yield for different locations and solar technologies. The data sets used cover 1 year and are taken from four different locations with different climate zones. These locations where Singapore (fully humid equatorial), Denmark (fully humid, warm temperature), Colorado (cold, arid) and Santa Catarina, Brazil (humid subtropical oceanic climate with hot summer).

Wilko Jessen et al. (2018) [36] discusses the importance of reference solar irradiance spectra for comparing and rating solar technologies, such as photovoltaic cells. IEC 60904-3 and ASTM G173 standards provide widely accepted reference spectra. However these standards may not accurately represent various atmospheric conditions and tilt angles found at different locations. To address this, the authors propose additional subordinate standard spectra related to eight sets of atmospheric conditions and tilt angles. These spectra can improve the accuracy of quick efficiency estimations when used instead of the IEC/G173 spectra. The applicability of these spectra has been confirmed at five test sites, based on average atmospheric aerosol optical depth and precipitable water vapor. The development of subordinate spectra for Direct Normal Irradiance and concentrating solar power and concentrating PV

is also considered, but it requires more sets of atmospheric conditions for intuitive selection.

In section 4.3 [36] they highlight that atmospheric conditions cannot alone account fully for the spectral response variations in solar technology applications. Tilt angle is an important factor that is contributing to the spectral mismatch between a standard spectrum and a realistic site-specific average spectrum. The impact varies for different types of solar cells, a-Si cells seems to be more sensitive to tilt angle changes than poly-Si, mono-Si, CdTe and CIS cells under certain conditions. For the a-Si cells, a tilt angle change of 5° resulted in a spectral mismatch of 0.1 to 1% depending on the tilt value angle, while for the other cells CdTe, CIS, poly-Si and mono-Si the mismatch was below 0.2% per 5° change. Figure 2.14 shows the change in δ_{RS} based on the change in tilt angle. R_S is the broadband responsivity of a PV cell, which is obtained by weighting its spectral responsivity, R_λ, with a representative incident solar spectrum, E_λ. δ_{RS} is the proportional change in a solar device efficiency.

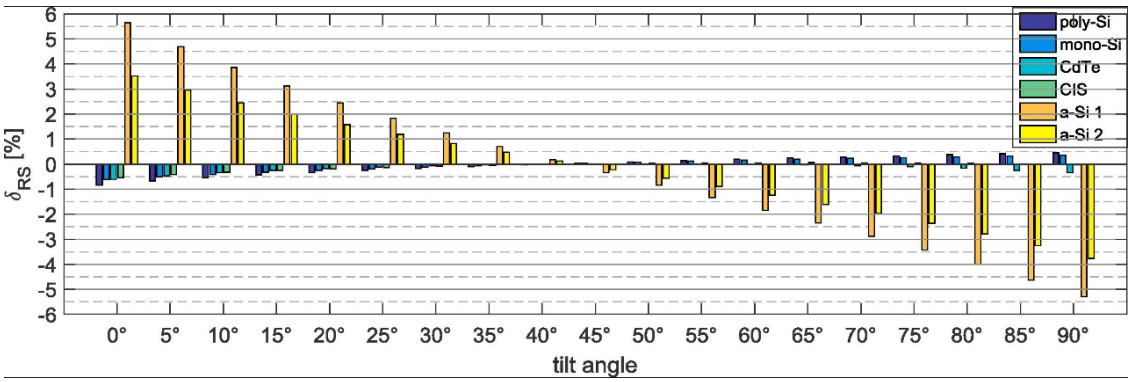

Figure 2.14: GTI spectral mismatch versus tilt angle for the IEC 60904 conditions. Source: W. Jessen, [36]

Takashi Minemoto et al. (2009) [37] sought to investigate and analyse the effects the spectral distribution of solar spectra and how it impacts the performance of PV modules outdoors, to do this the author needed an index. The author wanted to investigate if this can be done with APE. APE's uniqueness to the spectral irradiance distribution was analysed to confirm that a single APE value can define a solar spectrum's form. The author used a method similar to that adopted by the international electrotechnical commission to rate the spectral matching of a solar simulator to analyze the uniqueness of APE to the spectral irradiance distribution. The result showed that an APE value yielded a spectral irradiance distribution with a low standard deviation, which means that APE can be a suitable index to describe the spectral irradiance distribution for determining the outdoor performance of PV modules. The author was also able to find that the outdoor performance of crystalline silicon PV modules was mainly dependent on module temperature, while that of amorphous Si PV modules mainly depended on APE.

Shota Yoshida et al. (2013) [38] sought to estimate the nationwide output energies of photovoltaic modules in Japan using meteorological data from the Japan meteorological agency and the performance of PV modules. To estimate the output energy of PV modules, global tilted irradiance is required, but only global horizontal irradiance data are typically available in the Japan meteorological agency. Therefore, GTI was estimated from GHI using separation methods, and the optimum installation angle was used as a tilt angle at each location. The output energies of four types of PV modules were estimated using their performance and the estimated GTI. The table from the article shown in figure 2.15 2.15 shows the estimation of GTI, energy output, the module temperature and the APE of each PV module found in this study. The energy output in this study was estimated by multiplying the contour maps

of GTI in each year and the contour maps of performance ratio.

Site	Wakkanai	Sendai	Tokyo	Kofu	Nagoya	Hikone	Fukuoka
Latitude	45°24.9′N	38°15.7′N	35°41.4′N	35°40.0′N	35°10.0′N	35°16.5′N	33°34.9′N
Longitude	141°40.7′E	140°53.8′E	139°45.6′E	138°33.2′E	136°57.9′E	136°14.6′E	130°34.9′E
Tilt angle (°)	34.8	34.5	32.8	33.7	32.5	27.0	26.1
GTI (kWh/m^2)	1207	1377	1420	1666	1563	1447	1401
mc-Si (kWh/kWp)	945	1092	1108	1276	1199	1137	1091
tandem (kWh/kWp)	934	1063	1093	1248	1180	1130	1097
a-Si (kWh/kWp)	1044	1225	1269	1465	1383	1304	1271
3stack (kWh/kWp)	992	1159	1193	1381	1299	1223	1186
APE (eV)	1.921	1.923	1.925	1.920	1.923	1.929	1.931
mc-Si T_{mod} (°C)	24.5	30.7	34.4	35.9	35.8	33.7	36.0
Tandem T_{mod} (°C)	32.1	39.1	42.9	45.4	44.8	42.1	44.4
a-Si T_{mod} (°C)	26.0	31.9	35.2	36.8	36.6	34.5	36.5
3stack T_{mod} (°C)	23.0	28.8	32.2	33.5	33.5	31.7	33.8

Figure 2.15: Table from the article by Shota Yoshida [38]

The results from [38] demonstrate that the use of environment and performance contour maps in conjunction with the Japan meteorological agency's meteorological data is useful for estimating the output energy of the PV modules around Japan. When estimating the energy output for the PV modules, the effects of temperature solar spectrum was taken into consideration. With meteorological data it was possible to estimate energy output in any location by considering environmental factors. Therefore it was concluded that this this proposed method for the evaluation of the output energy for the PV modules can be useful for energy rating.

Chapter 3

Methodology

This chapter will address the methodology of this thesis. It will start the location of where the data has been measured, then mention which PV modules has been used for the comparison and how the EQE values for the individual PV module has been obtained. This will be followed by how the data processing of the spectral data has been conducted.

3.1 Location

The data used in this thesis were measured in southern Norway, Grimstad, recorded by stationary broadband Spectrafy instruments located on the roof of the university of Agder. Three Spectrafy instruments collects the global horizontal spectral irradiance, global tilted spectral irradiance and direct normal spectral irradiance. This data is measured in $\mathrm{W/m^2 \cdot} nm$.

Figure 3.1: The location of University of Agder in Grimstad at which the data is taken from, indicated by the red pin. Source: google maps

Table 3.1: Details for the spectral irradiance data

Latitude	58.33°
Longitude	8.58°
Start wavelength	280 nm
End wavelength	4000 nm
Start month	February 2020
End month	December 2021

3.2 PV modules

This thesis will compare four different PV modules using different technologies. These are the IBC MonoSol 305 VL5 (c-Si) [39], U-EA Type 100 (a-Si) [40], TS-Suite100 WS (CdTe) [41] and Solibro SL2-F (CIGS) [42]. The c-Si module and the CIGS module are modules that is being used on the roof of UiA, however they do not have EQE measurements for the different PV modules. This means they need to be acquired by other means, this will be explained in section 3.3.

3.3 Obtaining EQE values

The external quantum efficiency varies depending on the PV technology, this means four separate lists of spectral EQE representing the four PV technologies is needed. First, curves representing the individual PV types is found through data sheets and articles. Figure 3.2 is the curve used for the c-Si module, figure 3.3 is the curve used for the a-Si module, figure 3.4 is the curve used for the CdTe module and figure 3.5 is used for the CIGS module. To extract the data from these curves a tool, "WebPlotDigitizer", was used. It is a web based plot digitizer that can be freely accessed [43]. By downloading an image of graphs representing the EQE for these PV technologies and use the WebPlotDigitizer it is possible to create a list with the EQE as a function of wavelength for these PV technologies. The figures below shows the different graphs the EQE values were taken from.

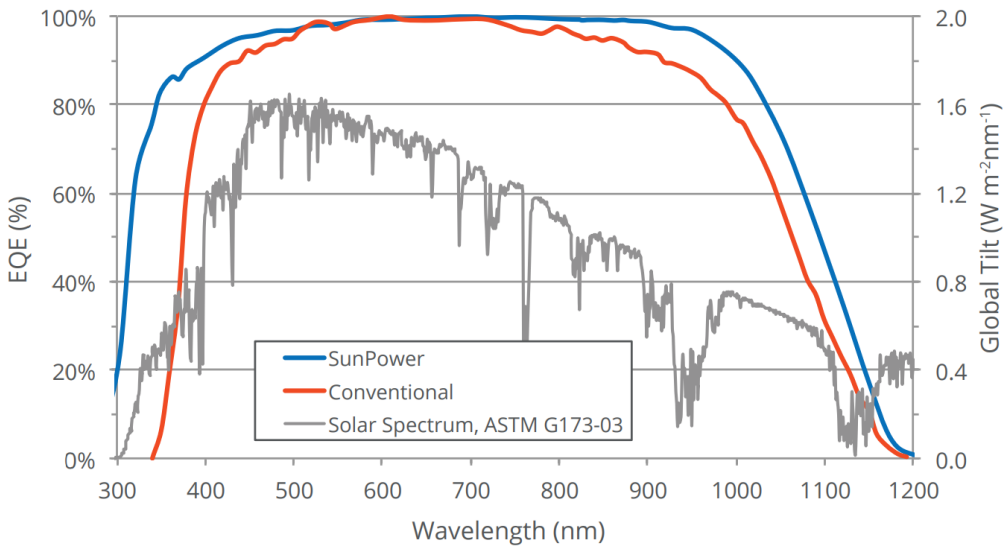

Figure 3.2: c-Si, the EQE values are taken from the blue line. Source: us.sunpower.com [44]

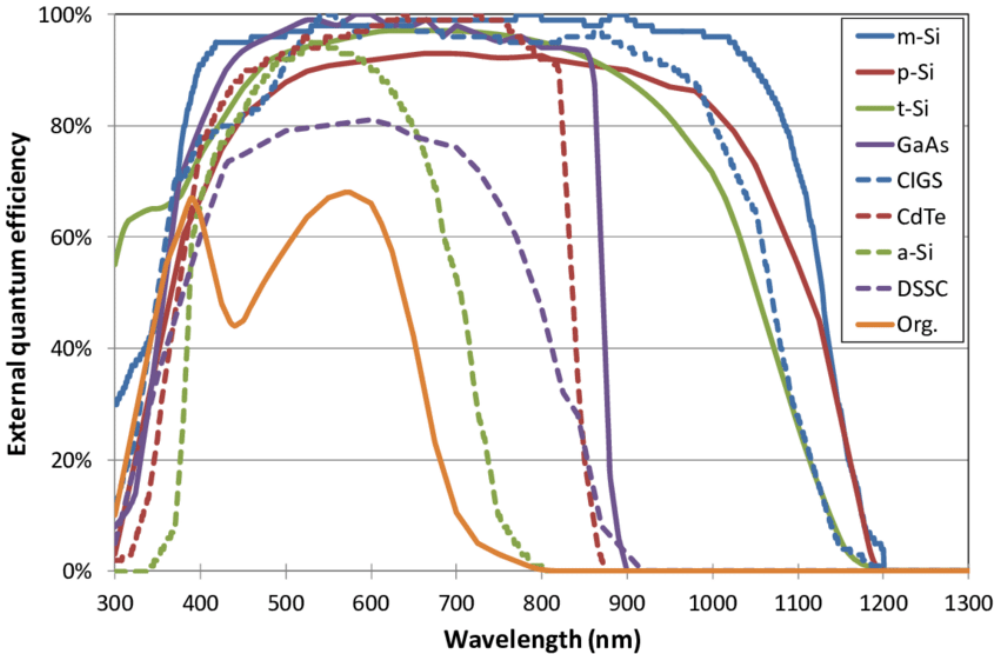

Figure 3.3: a-Si, the EQE values are taken from the striped green line. Source: B. Minnaert [45] page 7

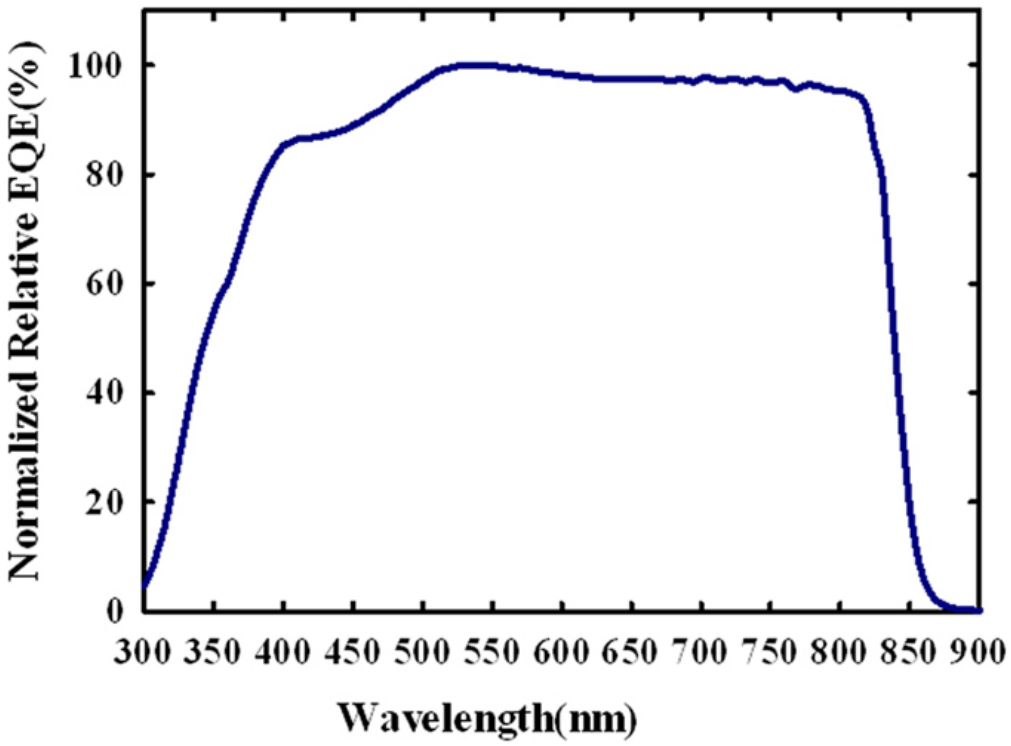

Figure 3.4: EQE graph for CdTe. Source: H. Dang and V. P. Singh [46]

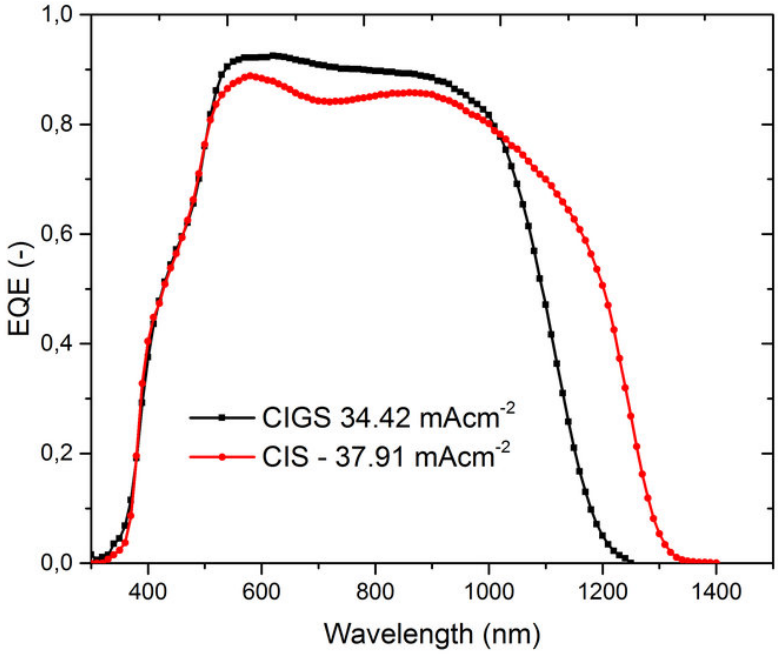

Figure 3.5: CIGS, the EQE value is taken from the black line. Source: R. K. Kothandaraman [47] page 67

3.4 Data processing

The data for this thesis has been processed through a python script B were the data is split into 2 years, each year is divided into each month, each month into each day and each day into every minute. The measurements starts at sunrise and ends on sunset. The file for January 2020 did not have data for global horizontal spectral irradiance and both May 2020 and August 2021 where missing. March, May, June, September, October and November in 2021 have some days missing. Two scripts were made, the first one calculates the total irradiance, photon flux, APE and W/h for both horizontal and tilted measurements for every minute. The second script calculates the average value for each wavelength in a month.

The first script calculates the total irradiance of each minute by reading the intensity of each λ and then, using the simpson function in python, integrates over the given λ range, which in this case are from 300 - 1200 nm. This interval is chosen since the EQE interval for c-Si goes from 300 - 1200 nm, this means any irradiance with photons outside this range will not be absorbed by the module. The photon flux is then calculated using the total irradiance for the minute utilizing the equation 2.5. APE is calculated with the use of equation 2.4. Furthermore, W/h was calculated by multiplying total irradiance with 1/60.

The second script C was made by creating an empty array for the sum of GHI and GTI values with counters set for the number of minutes with GHI and GTI data. The script loops through each minute of each day in a month. It will then store the GHI and GTI value for each wavelength. The script will then calculate the average value for each wavelength for the month and store it in a data frame. This data frame can then be called upon to create a spectral distribution graph for the average GHI and GTI for all months.

The calculated energy production for all four PV panels is based on the average values of a

month. The calculation of c-Si in month of February 2020 can be used as an example. First the total irradiance for both GH and GT (kWh/m^2) for the month of February is summed. Since c-Si operates within the wavelength of 300 - 1200 nm 3.2, any light outside of this range can be disregarded for power production. The summed irradiance for February 2020 within the given wavelength range is 25.471 kWh/m^2 for the horizontal position and 50.320 kWh/m^2 for the tilted position.

By using the second script the average photon flux value for each λ in February is multiplied with the corresponding EQE λ. This will give the average number of electrons that is absorbed. The Isc is then calculated by multiplying the number of electrons absorbed for each λ with q (elementary charge) and then summed to get the total Isc. This will be the average Isc value for the month of February 2020.

Power density (Pmax, in kW/m^2) can be calculated using equation 2.9, although Isc is calculated from the irradiance from the data, Voc and FF is taken from STC on the data sheet of the respective PV modules that is being compared. As mentioned previously, temperature affects the value of Voc in particular, which in turn affects Pmax. Hence, the temperature of the cell needs to be accounted for, and this is done using equation 2.10. For the example month of February 2020, the monthly average cell temperature is 6.75 °C for GHI conditions and 10.16 °C for GTI conditions. The data sheet of each PV module provide the temperature coefficient of Pmax, this explains how much power is lost per °C. The average ambient temperature of February 2020 is 3.5 °C, and to get a more accurate estimate of Pmax taking temperature into consideration the equation 2.11 is used. As mentioned in section 2.1, peak sun light is identical to the average daily solar isolation. With the new temperature-corrected Pmax the energy density of a module can be calculated by multiplying Pmax with the Peak sun hours for the month. This process is repeated for every month in 2020 and 2021, except for the three missing months. The python scripts used in this thesis can be found in the appendix A and B.

The article by King [31] provides a table with different configurations for various types of modules and mounting. Using equation 2.12 and 2.13 with module type glass/polymer, open rack, and the recommended values a = -3.56, b = -0.075 and ΔT = 3 °C for the c-Si PV module for three example months in 2020 gave the results displayed in tables 3.4 and 3.4 below.

Table 3.2: GHI temperatures

Month	**Cell(°C)**	**Module(°C)**
June 2020	26.2	25.2
July 2020	22.7	21.8
August 2020	25.2	24.2

Table 3.3: GTI temperatures

Month	**Cell(°C)**	**Module(°C)**
June 2020	26.3	25.3
July 2020	22.1	21.2
August 2020	26.8	25.7

3.5 Data measurement equipment

This section will go through the measuring equipment used in this thesis, this will mainly encompass the equipment used for the comparison of the portable spectrometer.

3.5.1 Stationary Spectrometer SolSIM-D2

SolSIM-D2 is a spectral irradiance sensor from Spectrafy that measures global solar spectral irradiance from 280 to 4000 nm. It uses filtered photodiodes to make precise, multi-spectral measurements of the solar spectrum in several narrow wavelength bands. These measurements then inform the SolarSIM-G's software to resolve the complete global solar spectrum and total global irradiance, under all sky conditions. [48]

Figure 3.6: SolSIM-D2 [48]

3.5.2 Portable Spectrometer

A high-speed miniature fiber optic spectrometer HR2000+ is used as a portable instrument to measure solar spectra. It is responsive to wavelengths from 200 to 1100 nm. Inside the spectrometer is a memory chip that saves calibration data, telling it how to measure the light.

Figure 3.7: HR2000+ Spectrometer [49]

Figure 3.8 is an inside view of the portable spectrometer HR2000+, showing the light's pathway and how it interacts with the spectrometer components. The HR2000+ spectrometer contains a charge coupled device (CCD) detector, a component that is highly sensitive to incoming photons. This detector is divided into several small, light-reactive areas known as pixels, which produces an image of the target scene. When these pixels are struck by a photon, it will be converted into one or more electrons. The number of electrons gathered is directly proportional with the intensity of the scene at each individual pixel. After measuring the number of electrons in each pixel during the CCD's clock-out period, the original scene

can be accurately recreated. [50] Connected to the spectrometer is a fiber optical cable. These cables carries light from one place to another. A cosine corrector is an optical diffuser that is placed on one of the ends of a fiber-optic cable in order to expand the angle at which light enters the cable to 180°. [50]

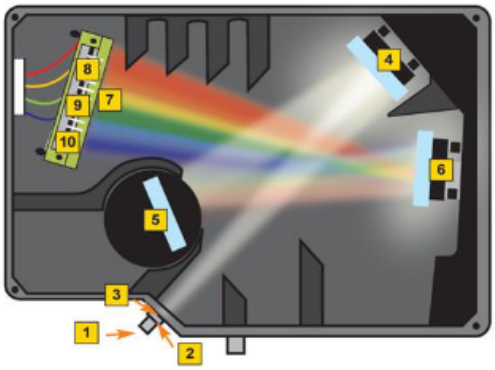

Figure 3.8: HR2000+ optical components on the light path. 1) SMA connector, 2) Entrance slit, 3) Long pass absorbing filter, 4) Collimating mirror, 5) Grating, 6) Focusing mirror, 7) L2 & L4 detector collection lenses, 8) Detector, 9) Variable long pass filter, 10) UV windows (quartz) [49] [50]

3.6 Spectrafy setup

The stationary spectrometers are station on the roof of UiA where they make continuous measurements. One measuring in the tilted plane and one in the horizontal plane. They are connected to their own Spectrafy software that analyses the data channels from 7 diode filters. They calculate full-ranged spectra from 280 - 4000 nm with a 1 nm resolution, and stores the data for each minute. Figure 3.9 and 3.10 shows the tilted setup and the horizontal set up respectively.

Figure 3.9:

Figure 3.10:

3.7 Experimental setup and data collection

Before the calibration can start, the instrument known as DH+2000 needs to warm up. The deuterium lamp for UV light requires 20 minutes of warm-up and the halogen lamp for visible light needs 40. The portable spectrometer is connected to a PC via a USB. A program called OceanView software is used for calibration, and an optic cable connects the spectrometer to the DH+2000. Protective glasses are recommended during operation. In OceanView, the "Spectroscopy Application Wizard" is used to select absolute irradiance for calibration. Deuterium lamp calibrates 200-410 nm wavelengths, while halogen lamp handles 350-1100 nm, it is important to note that only one lamp can be used at the time. The two calibration files are combined into one. The settings for calibration are shown in table 3.4. The final step is entering the fiber diameter, which is 3900 microns for this setup. [50]

Table 3.4: Calibration details, [50]

	Deuterium lamp	**Halogen lamp**
Warm up time	20 min	40 min
Wavelengths	Maximum 410 nm	Minimum 350 nm
Integration time	80 ms	80 ms
Scans to average	5	5
Boxcar width	5	5
Fiber diameter	3900 microns	3900 microns

Once the calibration files had been made, they were combined into one file, an option on tools under files in Oceanview. The program automatically chose the boundary wavelength to be 399.75 nm. [50]
The data collection with the portable spectrometer was done on the roof of UiA, first by placing the end of the fiber optic cable with cosine corrector on a 45° angle for the tilted measurements and then 90° for horizontal measurements. The integration time was set to automatic, scans to average was set to 5 and boxcar width was set to 5. Scans to average is a setting that reduces the noise and boxcar is a smoothing setting. The data would be processed through a script in python to create the graphs and calculate APE using equation 2.4 and 2.5 in order to compare the acquired data.[50]

As mentioned in the beginning this part of the thesis was not investigated further due to

problems with the calibration instrument. The deuterium lamp was not working properly, meaning the data within wavelengths below 350 nm were unreadable. This would not give sufficient data for the comparison of the stationary and portable spectrometers. One of the experiments that was that was conducted compare data for different sky conditions such as clear and cloudy days. Due to this setback, it was decided to change the focus of this thesis on the 2 years of spectral data that was provided by UiA.

Chapter 4

Results and discussion

In this section, spectral distribution graphs, tables for APE values and PV module performance results are presented. The results will be discussed as they are presented.

4.1 Spectral irradiance measurements

The raw data were inspected by examining and comparing spectral distributions for different time periods. Using 2 years of data a spectral distribution graph for almost all months for 2020 and 2021 were made, these graphs can be seen in appendix A. Figure 4.1 and figure 4.2 present irradiance spectra for two different days in the same month that show how the irradiance changes throughout the day from 11:00 to 15:00, one day with high levels of irradiance and another with low levels of irradiance. Note the difference in scale.

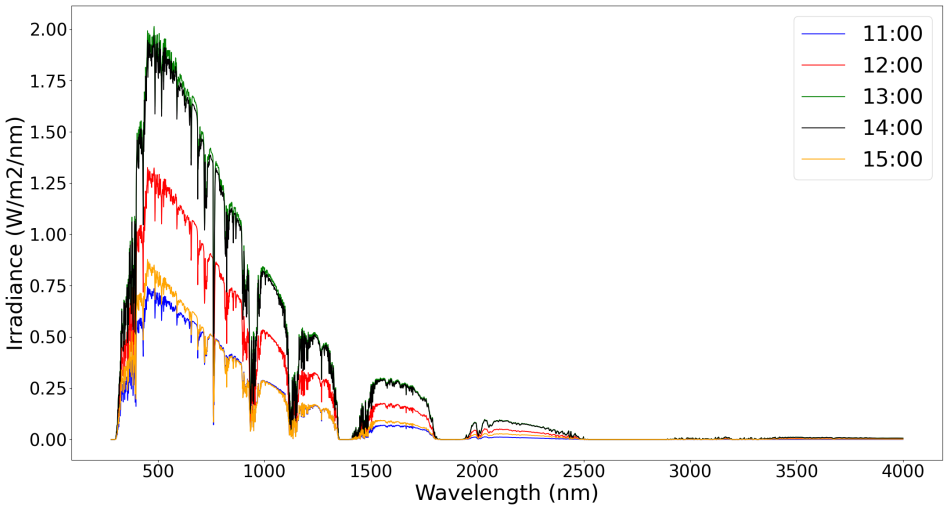

Figure 4.1: GHI spectral distribution at 12th of July

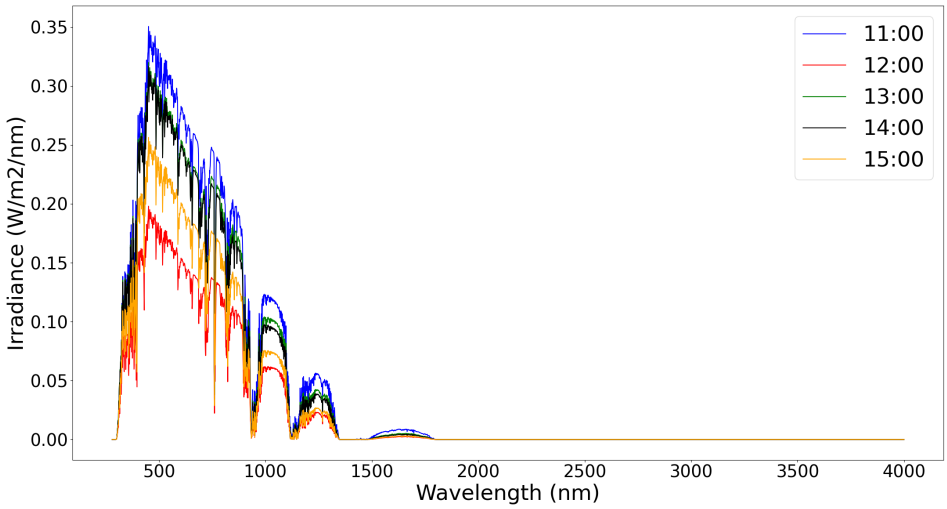

Figure 4.2: GHI spectral distribution at 18th of July

Figure 4.3 and 4.4 show the average spectral distribution for February 2020 and June 2020, respectively, illustrating the seasonal variation in spectral distributions. Appendix A contains the graphs for all months in the dataset.

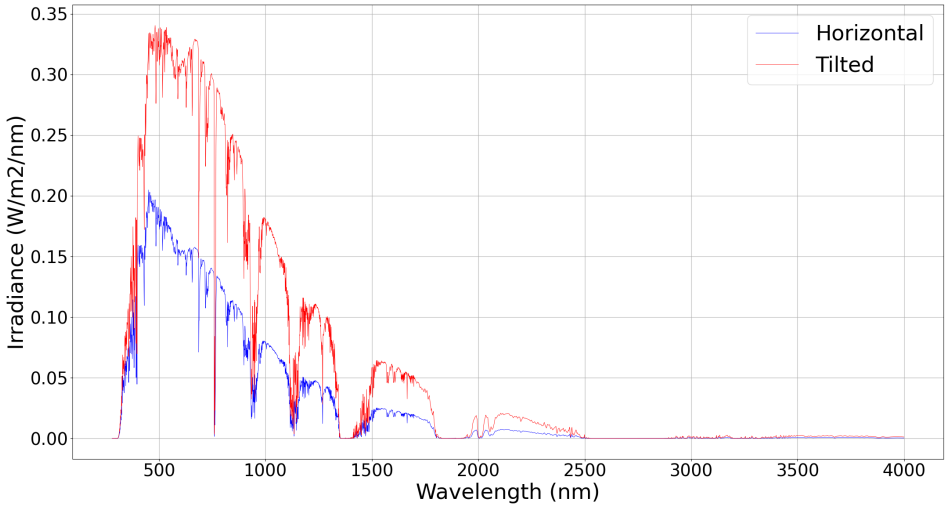

Figure 4.3: Average spectral distribution of GHI and GTI February 2020

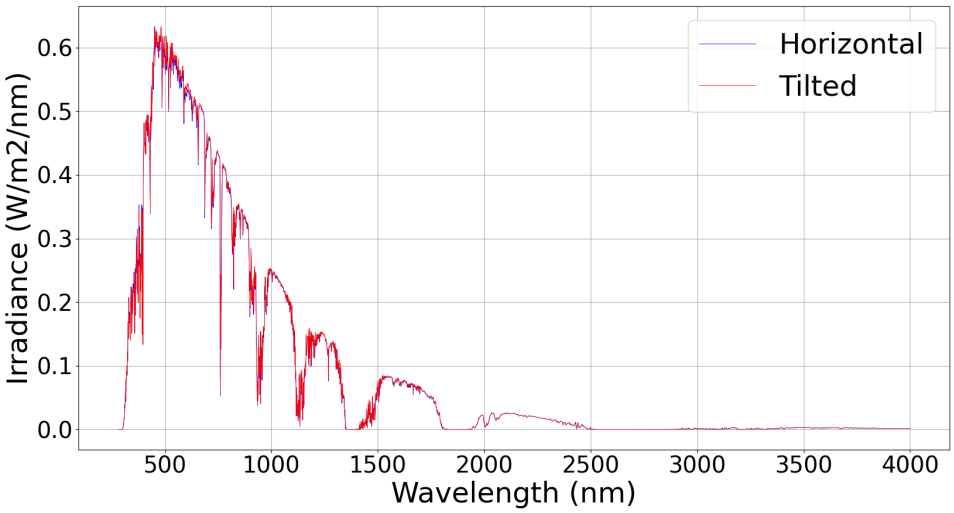

Figure 4.4: Average spectral distribution of GHI and GTI June 2020

Figure 4.5 and 4.6 show the average monthly irradiance for 2020 and 2021 respectively. This is based on the average value for each minute in the month from sunrise to sunset.

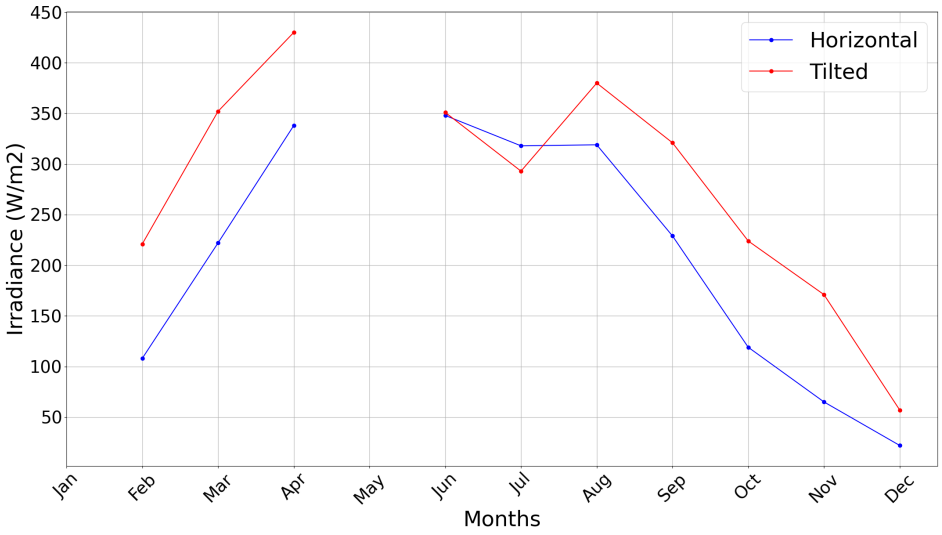

Figure 4.5: Average monthly GHI and GTI 2020

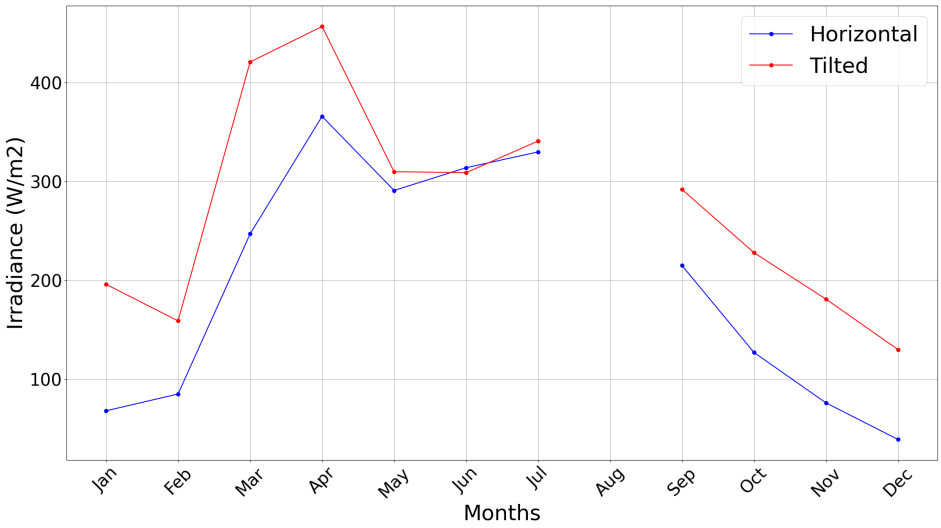

Figure 4.6: Average monthly GHI and GTI 2021

Figure 4.3 and 4.4 show how prominent the difference between the two angles are in the winter month and summer months. This is due the sun's position in the winter has a lower and shorter path then during the summer. This will in turn give less sunlight exposure to the horizontal angle. As seen in figure 4.3 the average peak for horizontal irradiance in February only reaches about 0.20 $W/m^2/nm$, while the average peak for tilted irradiance reaches upwards to 0.35 $W/m^2/nm$. This difference is minuscule in the summer months as seen in figure A.4, where both horizontal irradiance peak just over 0.6 $W/m^2/nm$. The spectral distribution graphs for all the months are in the appendix A.

Figure 4.5 and 4.6 show the average monthly irradiance for 2020 and 2021 respectively. There is a clear seasonal pattern in both GHI and GTI values. The irradiance is at its lowest in the winter months, increases in spring, reaches a peak in the summer months, and then decreases in the fall. This is of course expected due to the variation in sunlight intensity and duration through different seasons. However, due the missing data for several months in 2021, the 2021 graph looks somewhat strange. The 2020 graph looks relatively normal, except for the month of July where there is missing data for tilted irradiance.

4.2 APE values

The tables 4.2 and 4.2 present results for the monthly average APE value for both horizontal and tilted irradiance. The APE value has been calculated for the wavelength range 300 - 1200 nm. Figure 4.7 and figure 4.8 show how the monthly average APE varies over the 2 years.

Table 4.1: Monthly average APE value for 2020 for the 300 - 1200 nm range

Month	Horizontal Irradiance	Tilted Irradiance
February	1.86 eV	1.83 eV
March	1.85 eV	1.82 eV
April	1.84 eV	1.85 eV
June	1.85 eV	1.88 eV
July	1.86 eV	1.89 eV
August	1.86 eV	1.87 eV
September	1.86 eV	1.84 eV
October	1.87 eV	1.83 eV
November	1.89 eV	1.83 eV
December	1.92 eV	1.89 eV

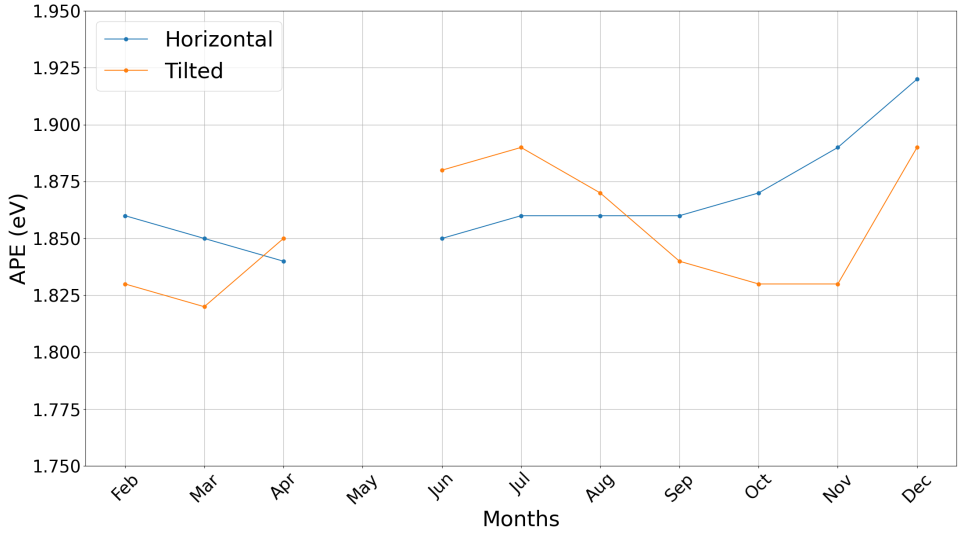

Figure 4.7: APE values for horizontal and tilted irradiance in 2020

Table 4.2: Monthly average APE value for 2021 for the 300 - 1200 nm range

Month	Horizontal Irradiance	Tilted Irradiance
January	1.87 eV	1.80 eV
February	1.89 eV	1.85 eV
March	1.83 eV	1.79 eV
April	1.82 eV	1.83 eV
May	1.86 eV	1.80 eV
June	1.86 eV	1.88 eV
July	1.85 eV	1.87 eV
September	1.86 eV	1.84 eV
October	1.87 eV	1.82 eV
November	1.87 eV	1.80 eV
December	1.90 eV	1.82 eV

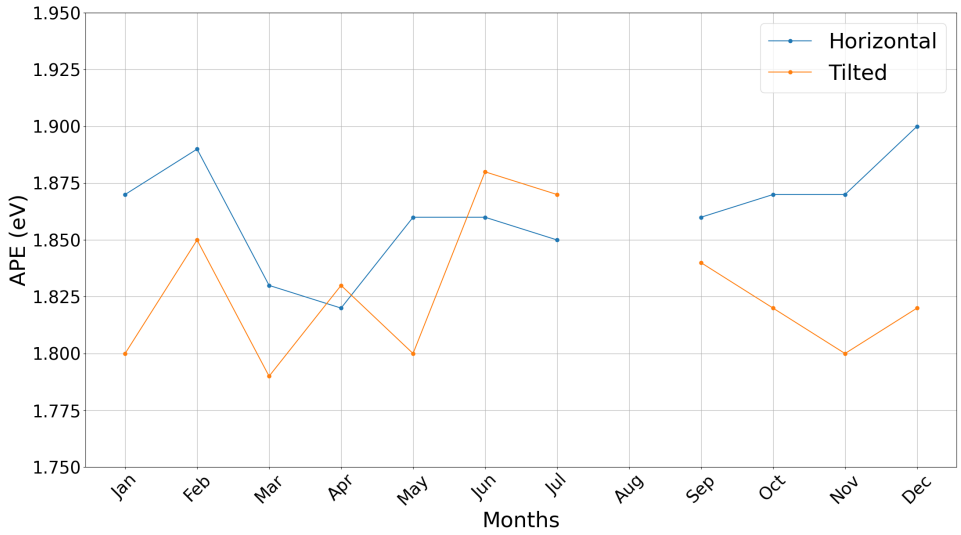

Figure 4.8: APE values for horizontal and tilted irradiance in 2021

4.3 APE results

Both 2020 and 2021 show a degree of seasonal variation in APE values. This variation is more noticeable in the tilted irradiance data. For example, in 2020, the APE value of tilted irradiance increases from February to July and then decreases towards December. However, the APE value sharply rises and peaks for December 2020, whereas, in 2021 the peak for tilted irradiance it is in June. This peak in December 2020 is highly unusual as the AM value is higher during winter months, which should decrease the APE value. For 2021 the APE value seems to be similar to 2020 as it is relatively lower in the winter and peaks in summer, but does not sharply rise in December. The APE value for horizontal irradiance for 2020 seems to hold a somewhat stable value for most of the year, but increases and peaks in December, which again is unusual. 2021 is also quite unusual as the APE values peaks in the winter months.

For most of the months, the APE values under tilted irradiance conditions are slightly lower than those under horizontal irradiance conditions. When comparing the same months across the two years, there is no consistent trend. Some months have higher APE values in 2020, while others have higher in 2021. This could be due to yearly variations in environmental factors such as atmospheric conditions, cloud cover, or other weather-related variables.

4.4 PV module energy production comparison

The comparison of the four PV modules will be split up into 8 different tables and 4 graphs. Each table will represent the PV module and its incidence angle (horizontal or tilted) and will span from February 2020 to December 2021. The tables consists of 7 columns each representing a different variable. These variables are: Month, PS hours(Peak sunlight hours), ambient temperature (°C), cell temperature (°C), short-circuit current (A/m^2), power density (W/m^2) and the energy density (kWh/m^2). The entire month of January 2020 was missing, so the table starts in February. As mentioned previously, the month of May 2020 and August 2021 is also missing. The STC variables from the data sheet of each PV module are also presented, these variables are: Vmpp (V), Impp (A), Voc (V), Isc (A), FF (calculated using equation 2.8) and the NOCT (°C) temperature.

The 4 graphs will be split into the GHI or GTI and year. They will show how the energy density of each PV module changes over the year in comparison to the others.

4.4.1 IBC MonoSol 305, c-Si

Table 4.3: Values taken from the PV modules data sheet [39]

Vmpp (V)	Impp (A)	Voc (V)	Isc (A)	FF	TC(Pmax) (%°C)	NOCT (°C)
32.6	9.36	40.2	9.87	0.77	0.42	46

Table 4.4: Horizontal angle, c-Si

Month	**PS Hours**	**Air(°C)**	**Cell(°C)**	**Isc(A/m^2)**	**Pmax(kW/m^2)**	**Energy(kWh/m^2)**
Feb 2020	25	3.5	7	46.4	1.328	33.827
Mar 2020	69	4	10	93.3	2.717	189.077
Apr 2020	120	7.2	17	136.6	4.092	492.429
Jun 2020	162	17.1	27	147.5	4.616	752.397
Jul 2020	148	14.8	24	135.21	4.175	620.011
Aug 2020	129	16.8	26	135.12	4.209	545.666
Sep 2020	75	13.4	20	97.34	2.955	222.890
Oct 2020	32	9.5	13	51.36	1.511	49.605
Nov 2020	13	7.4	6	28.00	0.810	10.749
Dec 2020	4	4.6	5	9.96	0.283	1.154
Jan 2021	13	-1.9	0	28.86	0.801	10.519
Feb 2021	15	-1.1	1	36.50	1.019	15.953
Mar 2021	52	4.6	12	103.39	3.027	157.736
Apr 2021	111	5.9	17	151.86	4.543	505.856
May 2021	91	9.9	18	122.61	3.698	339.162
Jun 2021	121	15.8	25	133.42	4.135	503.357
Jul 2021	153	18.2	28	140.08	4.392	673.994
Sep 2021	60	14.3	21	92.07	2.801	169.504
Oct 2021	32	10.4	14	54.76	1.620	52.489
Nov 2021	11	5.7	8	33.17	0.953	11.068
Dec 2021	6	0.4	1	17.04	0.476	3.315

Table 4.5: Tilted angle, c-Si

Month	**PS Hours**	**Air(°C)**	**Cell(°C)**	**Isc(A/m^2)**	**Pmax(kW/m^2)**	**Energy(kWh/m^2)**
Feb 2020	50	3.5	10	94.2	2.739	137.755
Mar 2020	108	4.0	14	147.5	4.370	474.817
Apr 2020	157	7.2	20	179.3	5.439	854.219
Jun 2020	164	17.1	28	148.9	4.659	765.289
Jul 2020	136	14.8	23	124.74	3.841	522.711
Aug 2020	153	16.8	28	161.38	5.064	779.577
Sep 2020	104	13.4	23	136.55	4.194	438.291
Oct 2020	59	9.5	16	96.18	2.868	171.577
Nov 2020	32	7.4	12	72.94	2.140	70.523
Dec 2020	9	4.6	6	24.35	0.695	6.495
Jan 2021	35	-1.9	4	82.69	2.334	83.088
Feb 2021	27	-1.1	4	67.24	1.898	52.710
Mar 2021	87	4.6	17	176.53	5.289	462.467
Apr 2021	141	5.9	20	193.84	5.873	828.497
May 2021	97	9.9	19	130.46	3.941	383.151
Jun 2021	119	15.8	25	131.64	4.073	488.066
Jul 2021	158	18.2	28	145.27	4.561	722.723
Sep 2021	81	14.3	23	124.93	3.838	311.090
Oct 2021	56	10.4	17	97.77	2.929	164.598
Nov 2021	26	5.7	11	77.92	2.273	59.264
Dec 2021	20	0.4	4	55.11	1.559	32.584

4.4.2 U-EA Type 100-120W, a-Si

Table 4.6: Values taken from the PV modules data sheet [40]

Vmpp (V)	Impp (A)	Voc (V)	Isc (A)	FF	TC(Pmax) (%°C)	NOCT (°C)
53.5	1.87	71	2.25	0.62	0.35	45

Table 4.7: Horizontal angle, a-Si

Month	**PS Hours**	**Air(°C)**	**Cell(°C)**	**Isc(A/m^2)**	**Pmax(kW/m2)**	**Energy(kWh/m^2)**
Feb 2020	18	3.5	7	19.94	0.822	15.001
Mar 2020	49	4	11	40.01	1.675	82.960
Apr 2020	85	7.2	17	59.14	2.535	217.884
Jun 2020	118	17.1	28	64.92	2.887	340.703
Jul 2020	107	14.8	24	59.51	2.611	280.860
Aug 2020	94	16.8	27	59.68	2.643	249.140
Sep 2020	54	13.4	20	42.69	1.850	100.921
Oct 2020	23	9.5	13	22.49	0.949	22.600
Nov 2020	9	7.4	9	12.13	0.505	4.848
Dec 2020	2	4.6	5	4.32	0.177	0.525
Jan 2021	9	-1.9	0	12.16	0.489	4.557
Feb 2021	11	-1.1	1	15.85	0.640	7.241
Mar 2021	37	4.6	12	44.31	1.864	69.047
Apr 2021	78	5.9	17	65.01	2.786	219.835
May 2021	66	9.9	19	53.68	2.314	153.128
Jun 2021	88	15.8	26	58.83	2.596	229.283
Jul 2021	111	18.2	26	61.73	2.729	303.973
Sep 2021	43	14.3	21	40.57	1.761	77.407
Oct 2021	23	10.4	14	23.93	1.015	23.769
Nov 2021	8	5.7	8	14.33	0.594	4.973
Dec 2021	5	0.4	2	7.29	0.294	1.474

Table 4.8: Tilted angle, a-Si

Month	**PS Hours**	**Air(°C)**	**Cell(°C)**	**Isc(A/m^2)**	**Pmax(kW/m2)**	**Energy(kWh/m^2)**
Feb 2020	34	3.5	10	37.61	1.571	53.968
Mar 2020	75	4	15	61.36	2.067	156.454
Apr 2020	111	7.2	20	76.86	3.334	371.135
Jun 2020	118	17.1	28	65.59	2.919	347.237
Jul 2020	91	14.8	23	55.17	2.414	220.416
Aug 2020	111	16.8	29	70.67	3.152	350.235
Sep 2020	74	13.4	23	58.45	2.559	190.003
Oct 2020	41	9.5	16	39.39	1.683	69.884
Nov 2020	21	7.4	13	27.45	1.156	25.221
Dec 2020	6	4.6	6	8.67	0.357	2.158
Jan 2021	22	-1.9	4	29.46	1.202	27.408
Feb 2021	18	-1.1	4	26.35	1.074	20.090
Mar 2021	60	4.6	18	72.61	3.117	188.074
Apr 2021	99	5.9	20	82.08	3.556	352.102
May 2021	69	9.9	19	56.88	2.456	171.575
Jun 2021	86	15.8	25	57.98	2.555	221.691
Jul 2021	114	18.2	26	63.71	2.819	322.906
Sep 2021	57	14.3	23	53.77	2.354	136.352
Oct 2021	38	10.4	18	39.94	1.712	66.657
Nov 2021	17	5.7	11	29.72	1.245	21.701
Dec 2021	12	0.4	4	18.49	0.755	9.823

4.4.3 TS-Suite100 WS, CdTe

Table 4.9: Values taken from the PV modules data sheet [41]

Vmpp (V)	Impp (A)	Voc (V)	Isc (A)	FF	TC(Pmax) (%°C)	NOCT (°C)
54.7	1.83	69.5	1.99	0.72	0.33	45

Table 4.10: Horizontal angle, CdTe

Month	**PS Hours**	**Air(°C)**	**Cell(°C)**	**Isc(A/m^2)**	**Pmax(kW/m^2)**	**Energy(kWh/m^2)**
Feb 2020	19	3.5	7	28.17	1.326	26.047
Mar 2020	53	4	11	56.32	2.688	143.407
Apr 2020	92	7.2	17	82.92	4.046	374.799
Jun 2020	127	17.1	28	90.77	4.587	583.263
Jul 2020	115	14.8	25	83.21	4.160	482.416
Aug 2020	101	16.8	27	83.33	4.194	425.314
Sep 2020	58	13.4	21	59.73	2.945	172.921
Oct 2020	25	9.5	13	31.55	1.517	38.858
Nov 2020	10	7.4	9	17.12	0.813	8.396
Dec 2020	3	4.6	5	6.13	0.287	0.917
Jan 2021	10	-1.9	0	17.35	0.797	8.020
Feb 2021	12	-1.1	2	22.29	1.029	12.513
Mar 2021	39	4.6	12	62.38	2.991	119.389
Apr 2021	85	5.9	17	91.47	4.462	379.756
May 2021	71	9.9	19	75.12	3.687	262.704
Jun 2021	95	15.8	25	82.26	4.124	392.582
Jul 2021	120	18.2	28	86.38	4.372	524.707
Sep 2021	47	14.3	21	56.75	2.802	132.529
Oct 2021	25	10.4	14	33.57	1.621	40.818
Nov 2021	9	5.7	8	20.25	0.957	8.625
Dec 2021	5	0.4	2	10.40	0.480	2.590

Table 4.11: Tilted angle, CdTe

Month	**(PS Hours)**	**Air(°C)**	**Cell(°C)**	**Isc(A/m^2)**	**Pmax(kW/m^2)**	**Energy(kWh/m^2)**
Feb 2020	37	3.5	10	55.02	2.621	97.692
Mar 2020	81	4	15	87.56	4.237	346.644
Apr 2020	120	7.2	21	108.16	5.335	640.774
Jun 2020	128	17.1	28	91.59	4.630	593.244
Jul 2020	98	14.8	24	76.94	3.837	377.502
Aug 2020	119	16.8	29	99.00	5.015	599.890
Sep 2020	80	13.4	23	82.66	4.115	329.957
Oct 2020	44	9.5	17	56.97	2.771	124.600
Nov 2020	23	7.4	13	41.51	1.993	47.548
Dec 2020	6	4.6	6	13.57	0.637	4.244
Jan 2021	25	-1.9	4	45.66	2.129	53.402
Feb 2021	20	-1.1	4	38.74	1.803	36.714
Mar 2021	65	4.6	18	104.18	5.213	332.841
Apr 2021	107	5.9	20	116.02	5.719	612.703
May 2021	75	9.9	20	79.67	3.916	294.793
Jun 2021	93	15.8	25	81.05	4.062	379.921
Jul 2021	123	18.2	29	89.30	4.526	558.644
Sep 2021	62	14.3	23	76.00	3.783	236.320
Oct 2021	42	10.4	18	57.80	2.821	118.986
Nov 2021	19	5.7	11	44.70	2.136	40.633
Dec 2021	14	0.4	4	29.80	1.390	20.053

4.4.4 SOLIBRO SL2-F, CIGS

Table 4.12: Values taken from the PV modules data sheet [42]

Vmpp (V)	Impp (A)	Voc (V)	Isc (A)	FF	TC(Pmax) (%°C)	NOCT (°C)
56.5	5.93	73.5	6.71	0.68	0.28	46

Table 4.13: Horizontal angle, CIGS

Month	**PS Hours**	**Air(°C)**	**Cell(°C)**	**Isc(A/m^2)**	**Pmax(kW/m^2)**	**Energy(kWh/m^2)**
Feb 2020	25	3.5	7	39.65	1882	48.910
Mar 2020	71	4	11	79.80	3835	272.638
Apr 2020	122	7.2	18	116.83	5722	703.109
Jun 2020	166	17.1	28	125.96	6356	1056.121
Jul 2020	151	14.8	25	115.33	5767	872.926
Aug 2020	132	16.8	27	115.43	5804	767.645
Sep 2020	76	13.4	21	83.20	4110	316.216
Oct 2020	33	9.5	13	43.86	2121	71.033
Nov 2020	13	7.4	10	23.91	1143	15.485
Dec 2020	4	4.6	5	8.44	399	1.655
Jan 2021	13	-1.9	0	24.62	1145	15.350
Feb 2021	15	-1.1	2	30.96	1146	23.053
Mar 2021	53	4.6	13	88.47	4269	227.215
Apr 2021	113	5.9	18	129.92	6362	723.370
May 2021	93	9.9	19	104.58	5144	481.225
Jun 2021	124	15.8	26	113.87	5707	708.181
Jul 2021	156	18.2	29	119.71	6049	946.798
Sep 2021	61	14.3	21	78.72	3894	240.233
Oct 2021	33	10.4	15	45.80	2271	74.952
Nov 2021	11	5.7	8	28.33	1349	15.975
Dec 2021	7	0.4	2	14.49	676	4.782

Table 4.14: Tilted angle, CIGS

Month	PS Hours	Air(°C)	Cell(°C)	Isc(A/m^2)	Pmax(kW/m^2)	Energy(kWh/m^2)
Feb 2020	51	3.5	11	81.95	3932	202.532
Mar 2020	111	4	15	127.20	6187	687.353
Apr 2020	160	7.2	21	153.87	7608	1220.672
Jun 2020	167	17.1	29	127.25	6423	1076.072
Jul 2020	128	14.8	24	106.32	5304	682.051
Aug 2020	157	16.8	29	138.45	7000	1099.676
Sep 2020	106	13.4	24	117.64	5861	625.647
Oct 2020	61	9.5	17	83.49	4077	249.618
Nov 2020	33	7.4	13	63.96	3089	104.426
Dec 2020	9	4.6	6	21.36	1012	9.704
Jan 2021	36	-1.9	4	72.65	3422	125.294
Feb 2021	28	-1.1	4	58.35	2745	78.061
Mar 2021	89	4.6	18	152.70	7489	669.727
Apr 2021	144	5.9	21	166.56	8234	1187.612
May 2021	99	9.9	20	111.57	5498	545.403
Jun 2021	122	15.8	26	112.56	5639	688.950
Jul 2021	161	18.2	29	124.53	6299	1018.189
Sep 2021	82	14.3	24	107.68	5364	444.012
Oct 2021	57	10.4	18	84.91	4158	239.250
Nov 2021	26	5.7	12	68.21	3281	87.675
Dec 2021	21	0.4	5	48.66	2293	49.220

Figure 4.9 shows the Energy density month by month for 2020 in the horizontal position. As mentioned previously the entire month of May was missing, so the value was extrapolated in the graph.

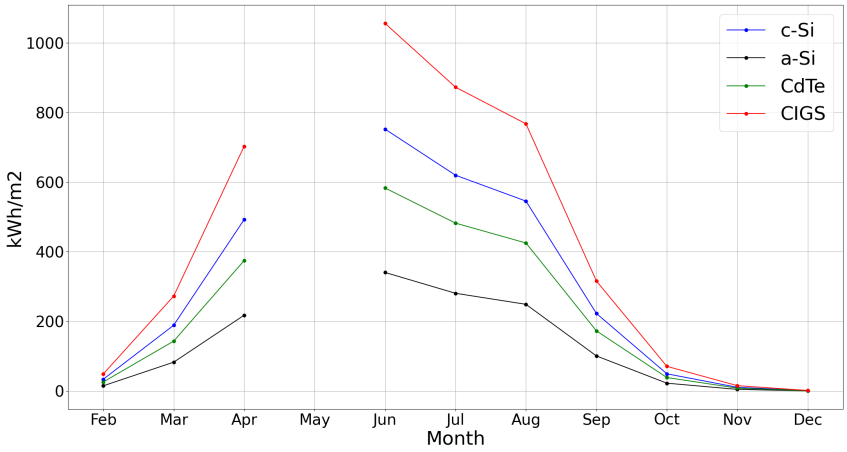

Figure 4.9: Horizontal energy production for all PV modules in 2020.

Figure 4.10 shows the power density month by month for 2021 in the horizontal position. There were several months in 2021 with data missing, these were: March from the 9th to the 13th, May from the 19th to the 26th, June from the 15th to the 19th, September from the 23rd to the 28th, October from the 9th to 11th and November from the 11th to the 19th. Just like May in 2020 the entire month of August were missing, so value of August was also extrapolated in the graph. However, since the all the modules are compared with the same data set should this comparison valid.

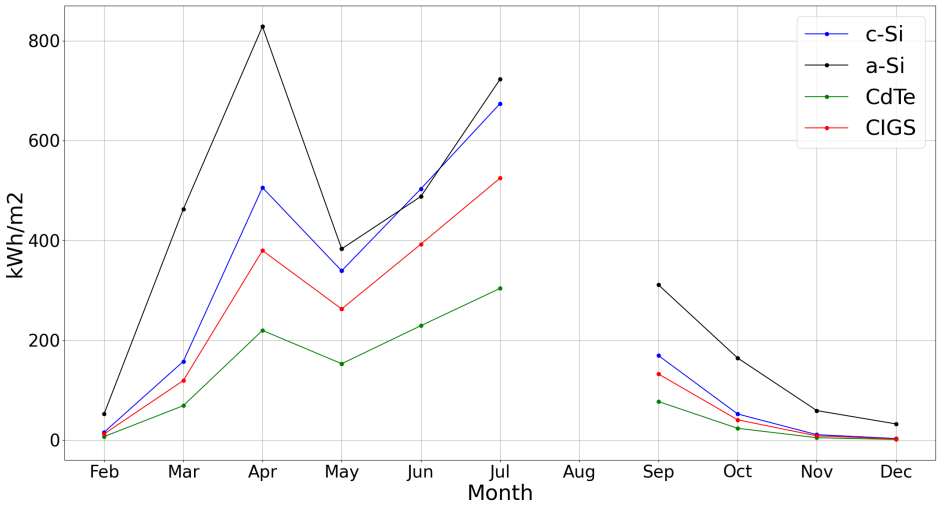

Figure 4.10: Horizontal energy production for all PV modules in 2021.

The only month in 2020 with missing data was July from the 21st to the 26th, but only for tilted irradiance.

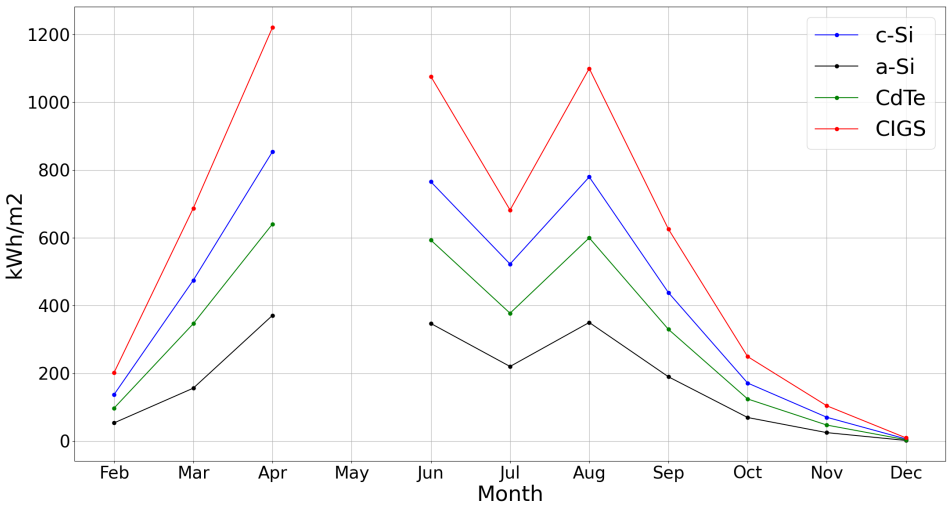

Figure 4.11: Tilted energy production for all PV modules in 2020.

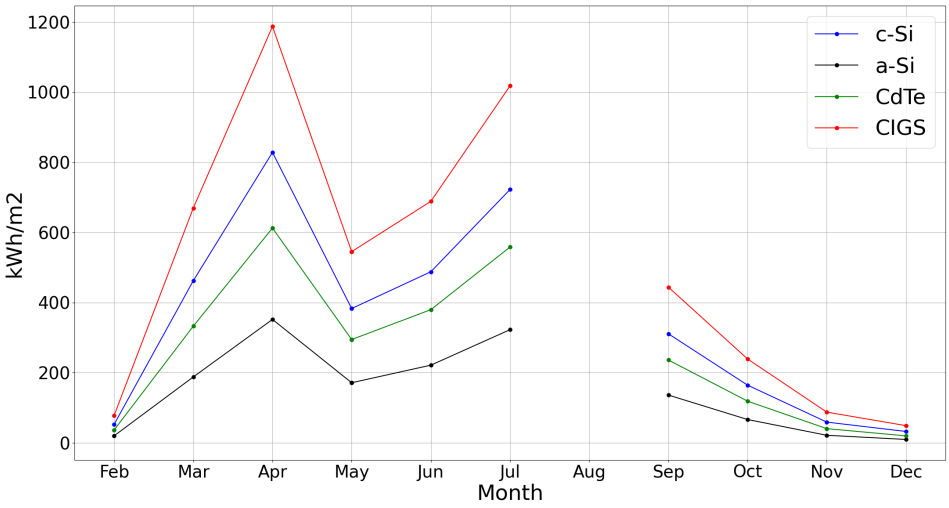

Figure 4.12: Tilted energy production for all PV modules in 2021.

4.5 Energy production

When observing the energy density values presented, they are incorrect. The energy density is more than the total GHI and GTI for most months. This is due to a mistake in the data processing section in the methodology. Using February 2020 as an example, the I_{sc} for this month is also calculated wrong as the actual I_{sc} is 37 A/m^2. This is just 10% of max I_{sc} per m^2 for a solar cell under STC [26], commercial solar cells have short-circuit currents between about 28 mA/cm^2 and 35 mA/cm^2 (280-350 A/m^2). This means the average irradiance (W/m^2) will also be equally low. The problem could be that since V_{oc} and FF were taken from the data sheet of the module, means that the areal need to be taken into account, and how the module is designed with the number of cells in series or parallel so the ratio between current and voltage is correct. 37 A/m^2 does not represent the current through a cell that is much smaller than one m^2. Assuming the cell is 15 cm $\times$ 15 cm, since the datasheet does not specify, the current produced by this cell is $37\,\mathrm{A/m^2} \times (0.15m)^2 = 0.8325\,\mathrm{A}$. If we assume that all the cells are connected in series, there will flow a 0.8225 A current through the module. This current can then multiply with 40.2 V (V_{oc}) and 0.77 (FF), this will give P = 25.77 W. To find W/m^2 the power needs to be divided by the area of the module, according to the datasheet [39], the area of the module is 1.64m^2, which would give a power density of 15.71 W/m^2. The energy density can be calculated by multiplying 15.71 W/m^2 with the number of hours that have been measured, which is 271 hours for February 2020. This means 15.71 W/m^2 $\times$ 271 hours = 4257 Wh/m^2. Due to time limitations, it is unfortunately not possible to change the results of the tables.

However, all the PV modules have been subjected to the same process, so the graph 4.9, 4.11, 4.10 and 4.12 should still be somewhat accurate in form, although the values in the y-Axis are wrong. The performance of the CIGS module is surprising as it is the highest-performing by far; it does have the largest range for photon absorption. However, CIGS modules only have a real-world efficiency of 10-12%. The other PV modules, on the other hand, do behave more as expected. The difference between a-Si to CIGS is 68.14%; for CdTe, it is 45.35%, and for c-Si, it is 29.27%. These "bumps" in the graphs are the missing data, which is quite evident when observing the graphs. When looking at table 2.15 from *Yoshida et al. (2013)* shows that the a-Si module produces more energy than the mc-Si module, which is not the case for this study. However, Yoshida's study takes place in Japan with different environmental

conditions than in Grimstad and uses a different method of determining energy output.

Table 4.15 and 4.16 shows the the increase in energy density from February to June for both 2020 and 2021.

Table 4.15: Percentage increase in GHI and GTI from February to June 2020 for different PV modules.

Module	**Energy density increase GH (%)**	**Energy density increase GT (%)**
c-Si	2124%	455%
a-Si	2171%	543%
CdTe	2139%	507%
CIGS	2059%	431%

Table 4.16: Percentage increase in GHI and GTI from February 2021 to June 2021 for different PV modules.

Module	**Energy density increase GH (%)**	**Energy density increase GT (%)**
c-Si	3055%	825%
a-Si	3066%	1003%
CdTe	3037%	934%
CIGS	2971%	782%

Evaluating the data using monthly average spectral distribution can provide a good insight into PV energy production. However, it has flaws, as it only gives a rough evaluation. By taking the average as mentioned previously, spectral distributions alone do not account for all the important factors that affect PV performance, such as temperature, angle of incidence, and system losses. Although the temperature was considered in this thesis, there were more accurate methods of obtaining temperature; NOCT only gives an approximate temperature since various factors can affect its accuracy. However, the method proposed by King (2004) [31] gives a more accurate temperature measurement since it also calculates module temperature. Therefore, while they can provide valuable insights, a more comprehensive approach to data analysis will generally provide a better evaluation of PV energy production. Furthermore, spectral distribution can vary considerably from month to month, depending on factors such as time of year and local weather patterns. Monthly average spectral distributions explain these variations and help understand how well a PV module will perform under different spectral conditions.

4.6 Future work

Several areas could have been interesting to conduct a further investigation on, but due to time limitations, this was not possible. This study analyzed the average APE values as a whole for a month without differentiating between wavelength ranges. A possible expansion is to make histograms of APE values for specific wavelength ranges. This could provide insights into how these values are distributed across different wavelengths in various conditions. Another area of interest could have been the comparison of the calculated temperature and the measured temperature of the PV modules. Using another method than NOCT to calculate the temperature of PV modules could have given a more accurate temperature value. One more idea is to test other types of PV modules, such as tandem. Using a different data set is also a possibility. Although the 2020 data set was missing two months, it only had holes in the other months except for July for tilted irradiance, unlike 2021, which had missing months and many holes in several months. This has made it difficult to work with. As mentioned in the literature review, the RISE method proposed by Erin E. Looney et

al. (2020) [35], a classification of spectral irradiance curve based on an iterative use of the k-means clustering algorithm, could have been an interesting topic to investigate.

Chapter 5

Conclusions

This thesis aimed to analyze two years of global horizontal spectral irradiance and global tilted spectral irradiance data to see how the spectral distribution changes over those two years and to estimate the energy output of 4 different types of PV modules using the provided spectral data. The initial aim was to test a portable spectrometer with the stationary broadband Spectrafy instruments by measuring incident sunlight at multiple angles and orientations. However, due to a defective calibration instrument, the primary focus was changed to analyzing the spectral data. The first thing that was done was to make the average spectral distribution graphs for each month in both the tilted and horizontal planes. It was interesting to see how much difference there is in irradiance, particularly for the horizontal plane. These monthly average spectral distribution graphs were made using this script C. The APE results did not have much to show for, tilted irradiance in 2020 showed some seasonal variation, while the rest did not so much. The APE analysis should have been done differently, as mentioned in further work, a histogram of APE values for specific wavelength ranges could have given a better analysis as it could tell .

Estimating the energy output of the four PV modules was done using both scripts B and C. This also needed the EQE values of the four different PV modules as they were not provided. Instead, they were obtained from PV module data sheets and articles. The values were extracted with the use of a tool called "WebPlotDigitizer" that can be freely accessed [43]. Once they had been acquired, could the script C be made. Unfortunately, the methodology for calculating the energy output is incorrect. As previously mentioned, the initial methodology did not take into account the area of the cell and how the module is designed. There was unfortunately not enough time to change to results presented in table 4.4.2 - 4.4.4. However, they have all been subjected to the same data processing, so the graphs: 4.9, 4.11, 4.10 and 4.12 could still reflect the truth. Although the CIGS module is surprising, its performance is much better than the others. The CIGS module does have a larger photon absorption range, but it does not have a high efficiency.

Appendix A

Appendix A

The figures below show the average monthly spectral distribution of GHI and GTI for 2020 and 2021. The spectral distribution of the months of January 2020, May 2020 and August 2021 are missing.

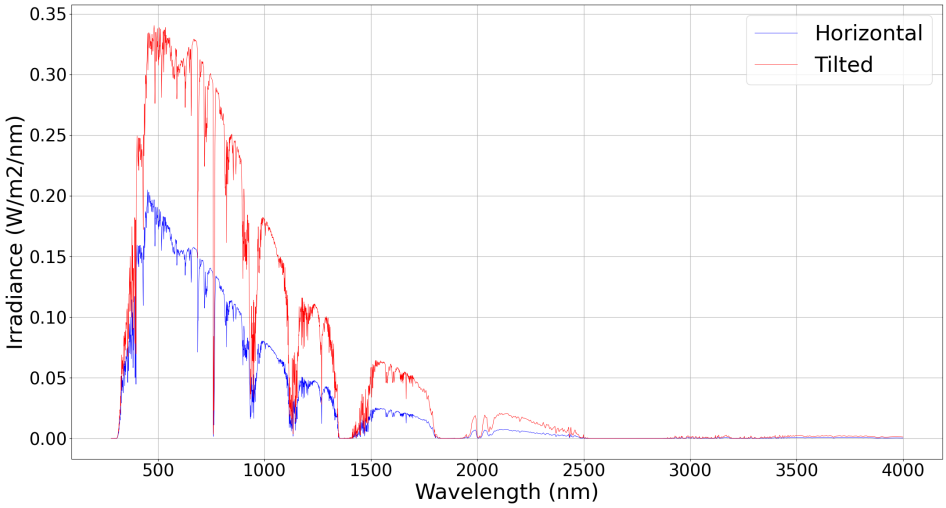

Figure A.1: Average spectral distribution for February 2020

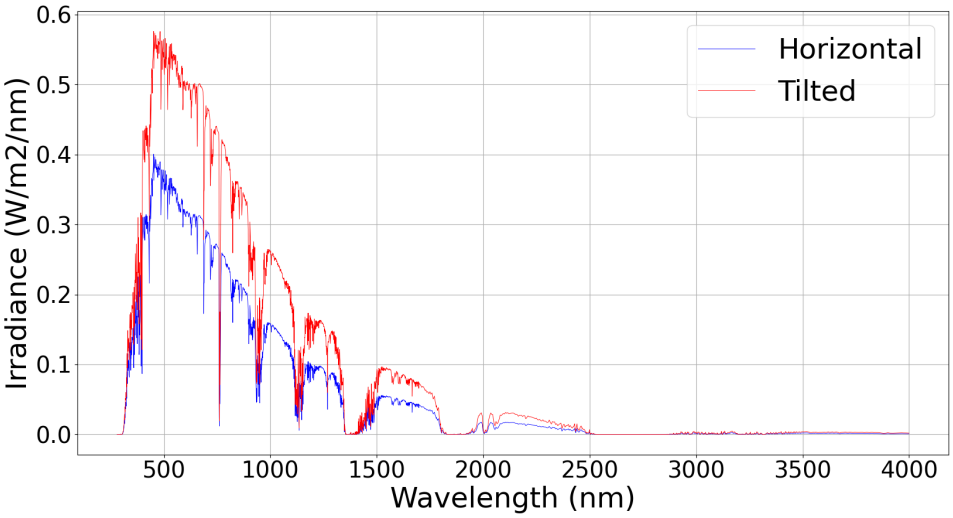

Figure A.2: Average spectral distribution of GHI and GTI, March 2020

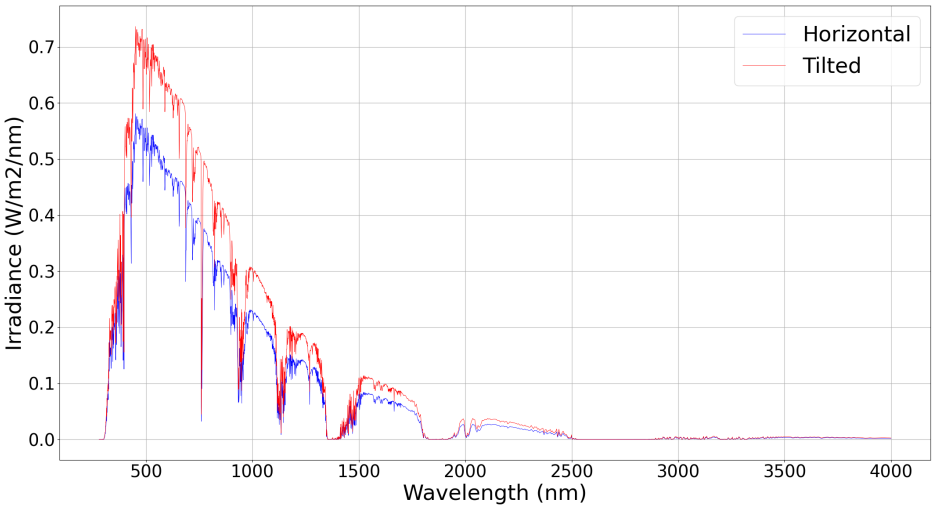

Figure A.3: Average spectral distribution of GHI and GTI, April 2020

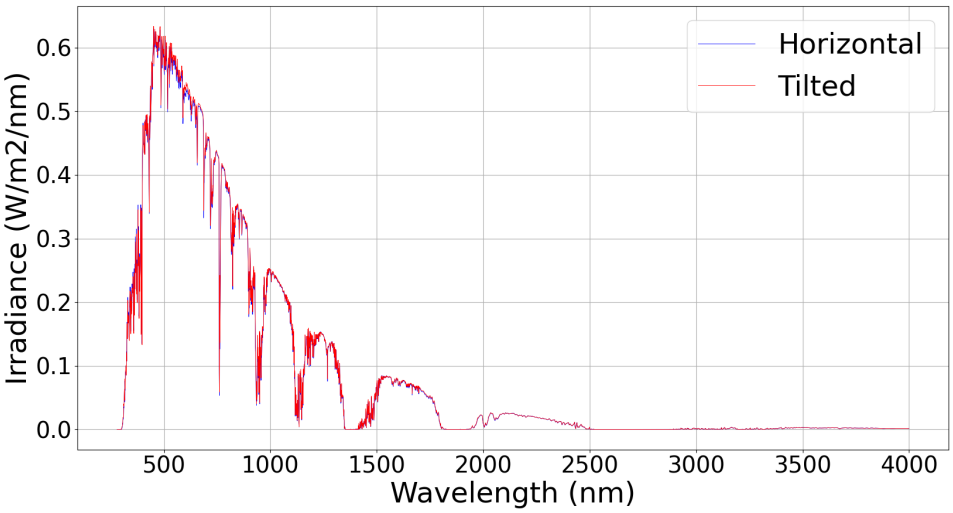

Figure A.4: Average spectral distribution of GHI and GTI June 2020

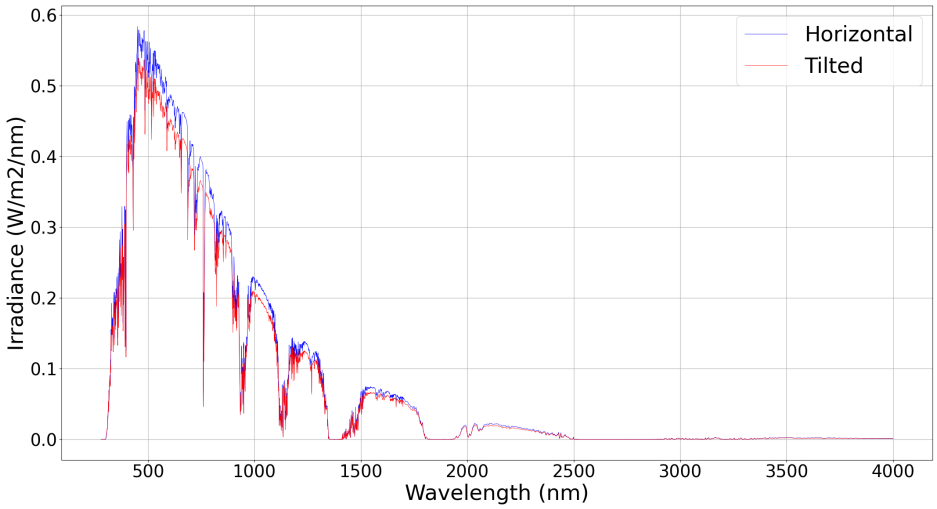

Figure A.5: Average spectral distribution of GHI and GTI, July 2020

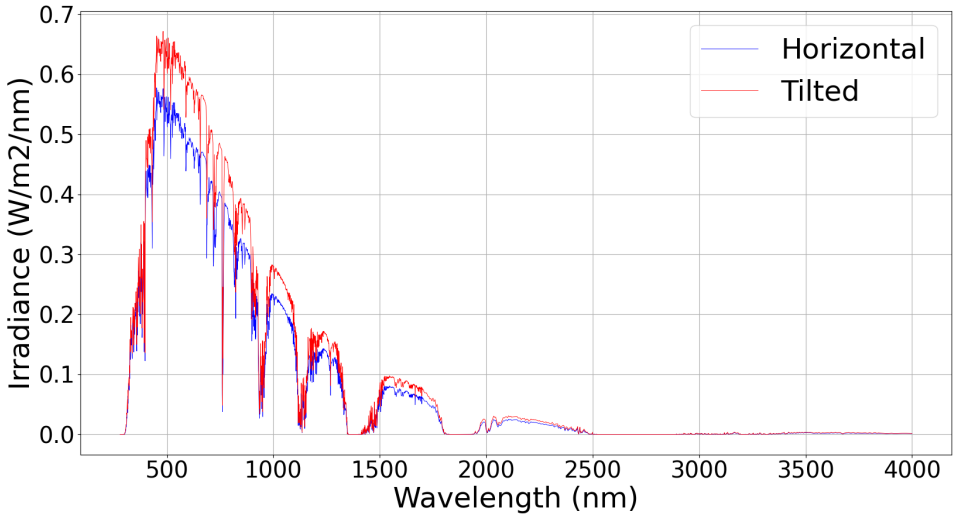

Figure A.6: Average spectral distribution of GHI and GTI, August 2020

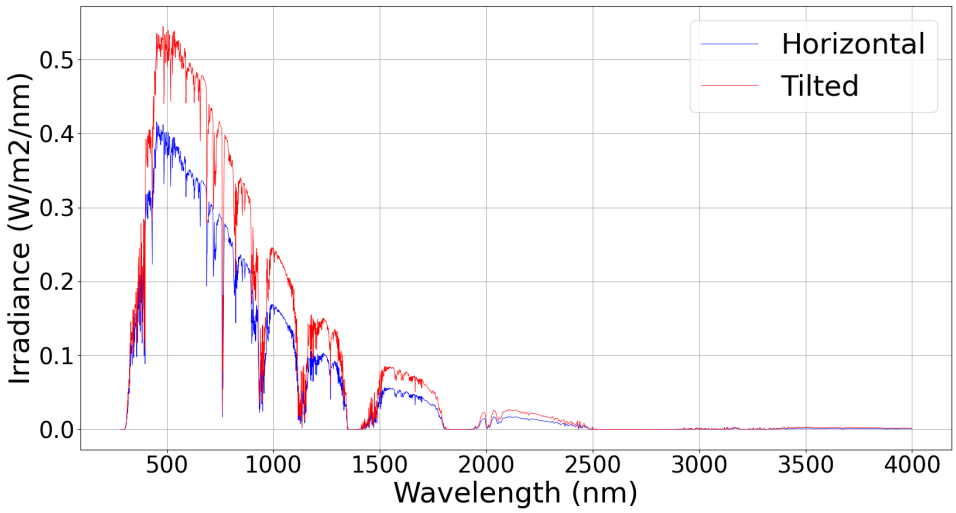

Figure A.7: Average spectral distribution of GHI and GTI, September 2020

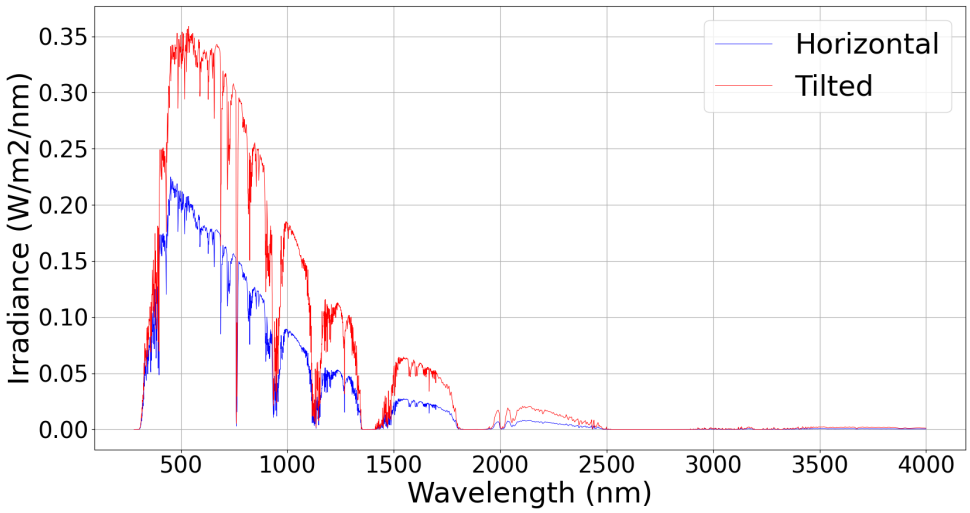

Figure A.8: Average spectral distribution of GHI and GTI, October 2020

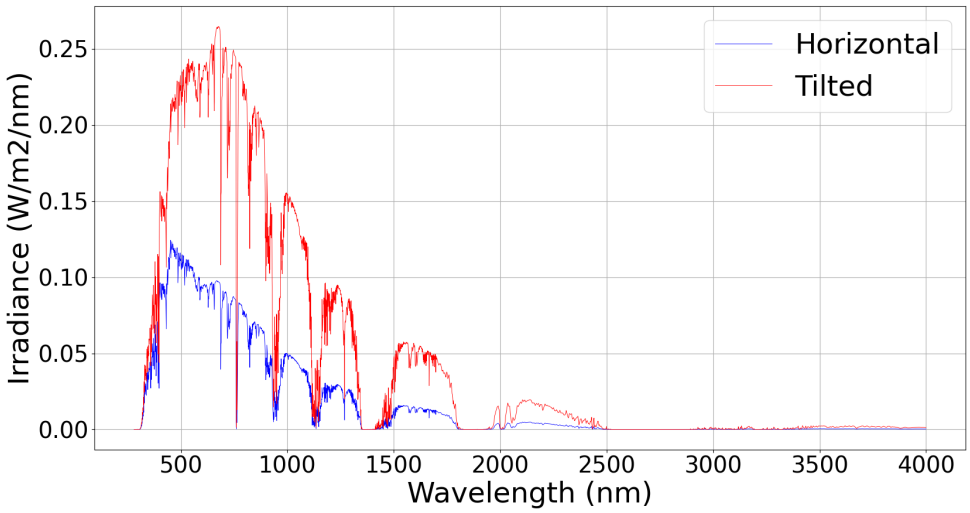

Figure A.9: Average spectral distribution of GHI and GTI, November 2020

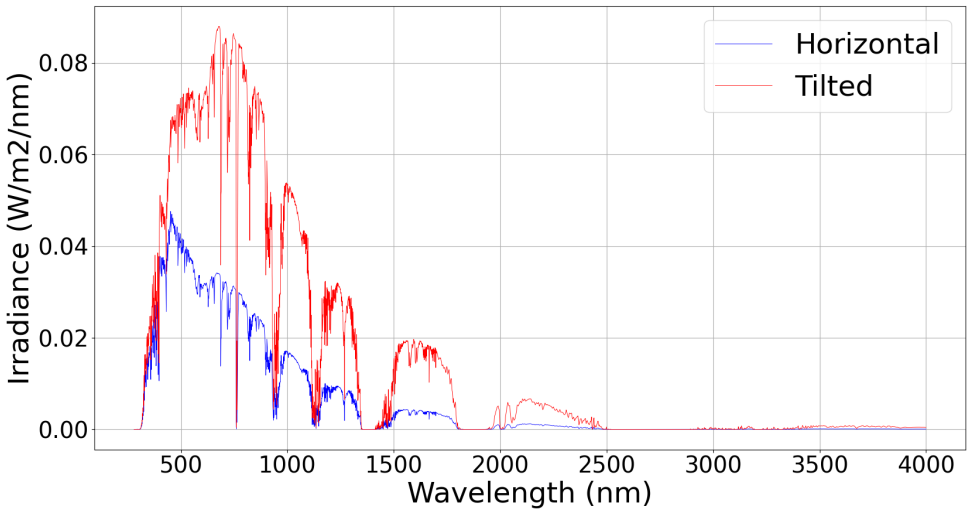

Figure A.10: Average spectral distribution of GHI and GTI, December 2020

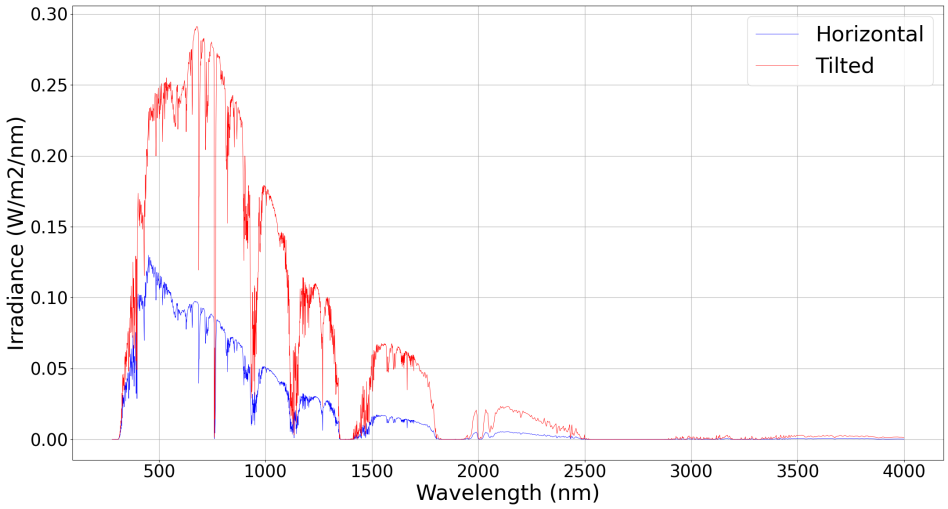

Figure A.11: Average spectral distribution of GHI and GTI, January 2021

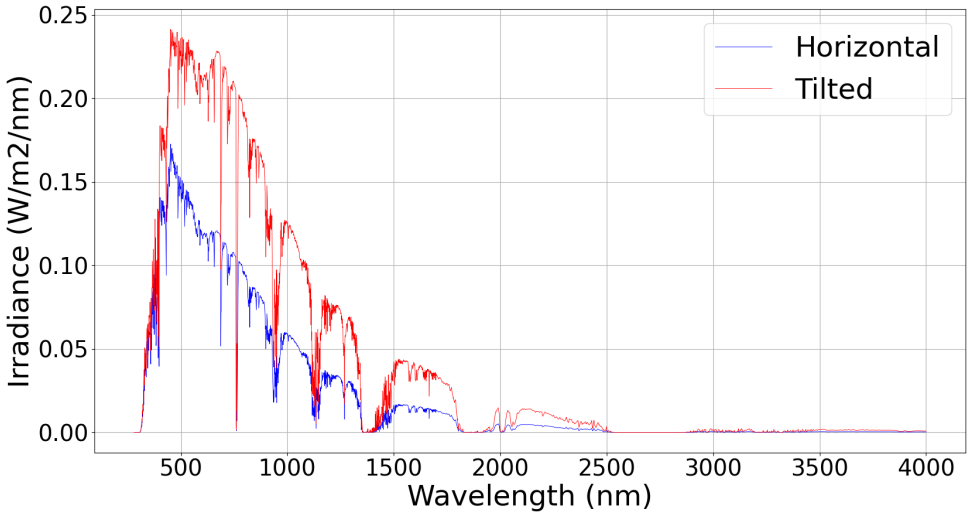

Figure A.12: Average spectral distribution of GHI and GTI, February 2021

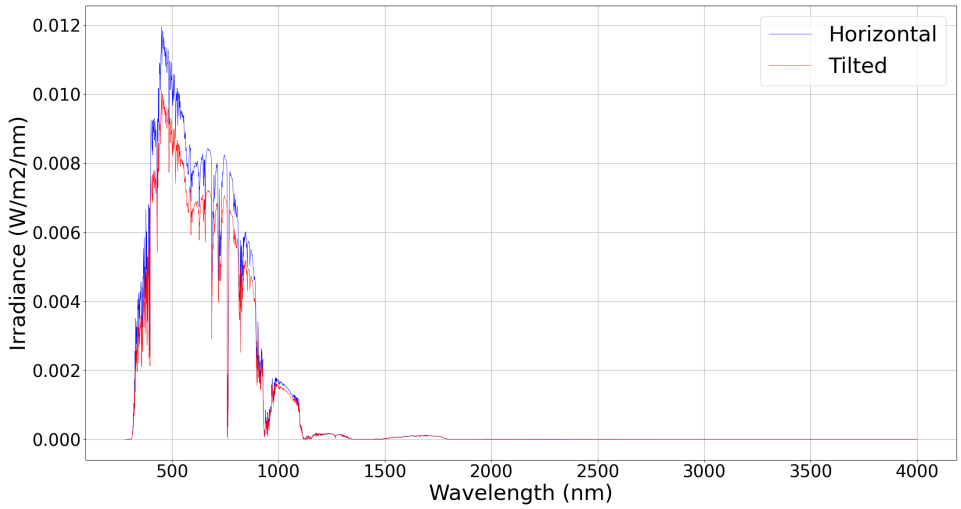

Figure A.13: Average spectral distribution of GHI and GTI, March 2021

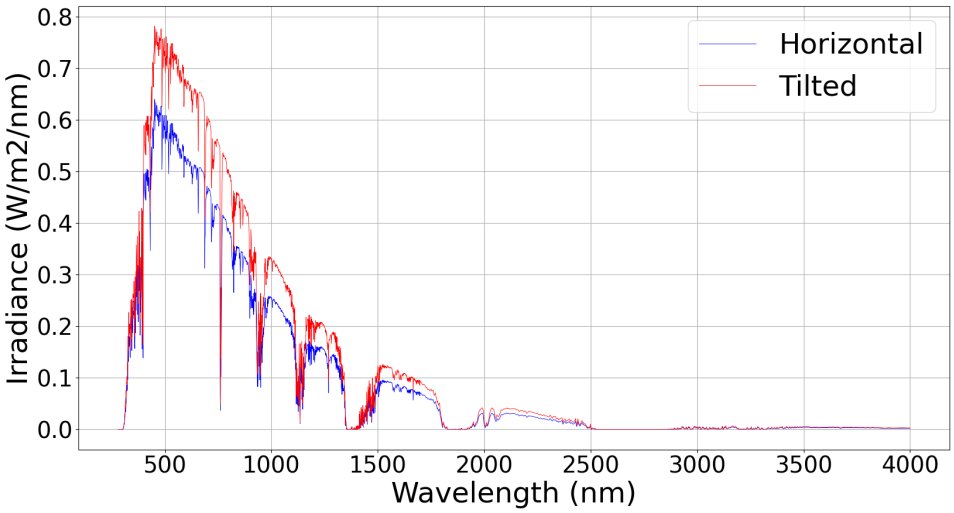

Figure A.14: Average spectral distribution of GHI and GTI, April 2021

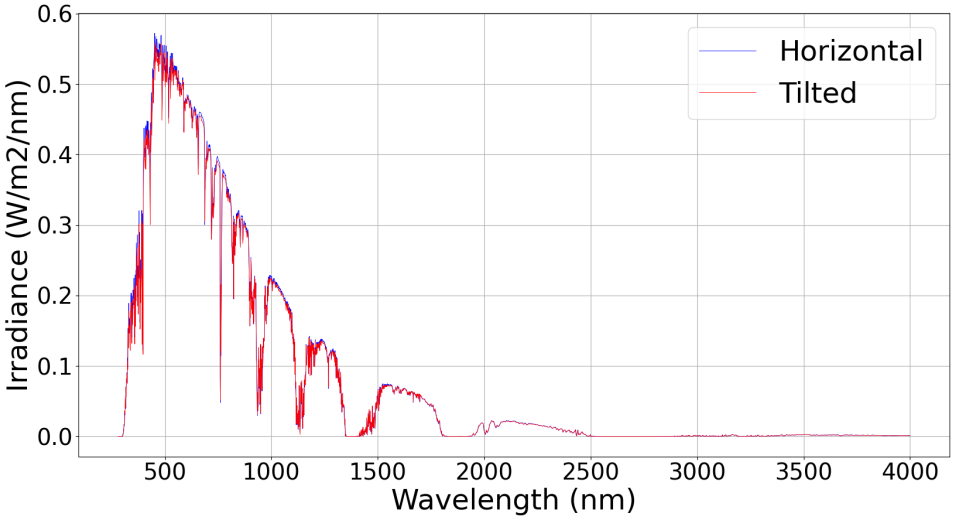

Figure A.15: Average spectral distribution of GHI and GTI, June 2021

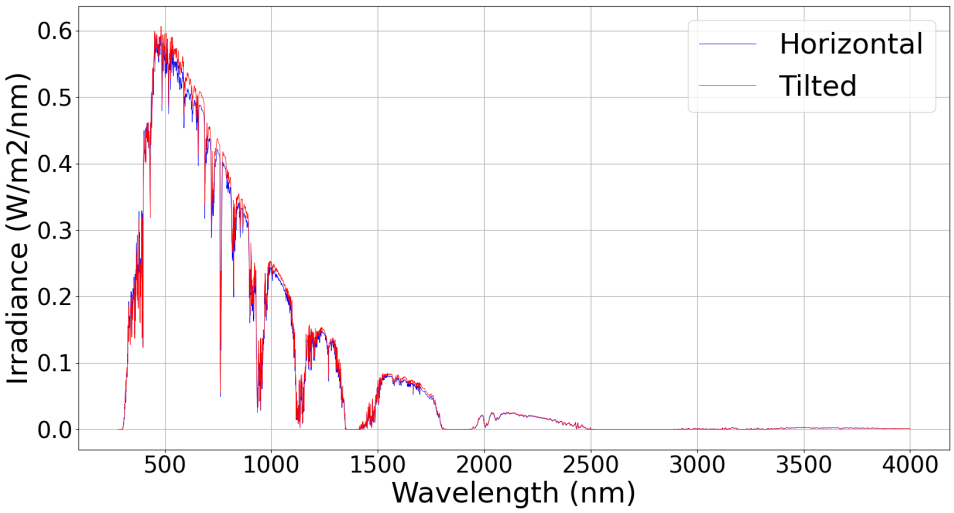

Figure A.16: Average spectral distribution of GHI and GTI, July 2021

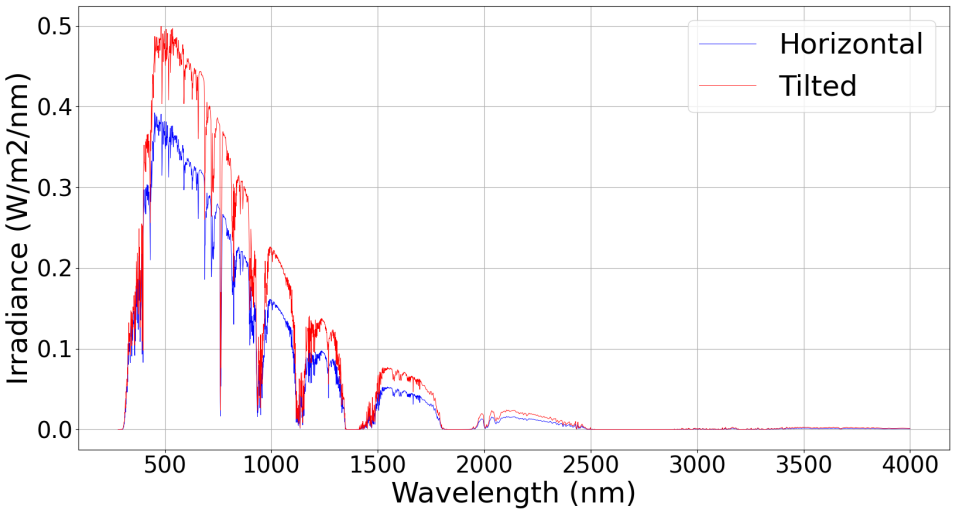

Figure A.17: Average spectral distribution of GHI and GTI, September 2021

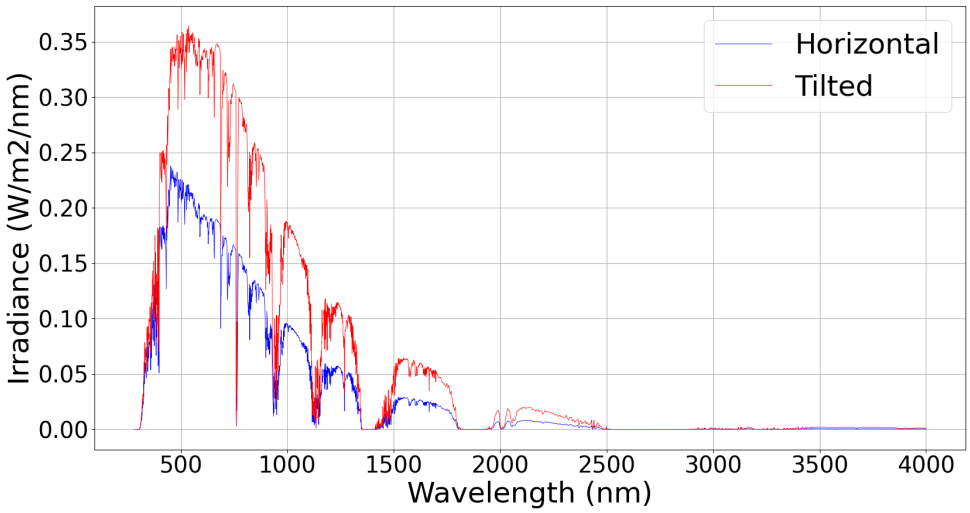

Figure A.18: Average spectral distribution of GHI and GTI, October 2021

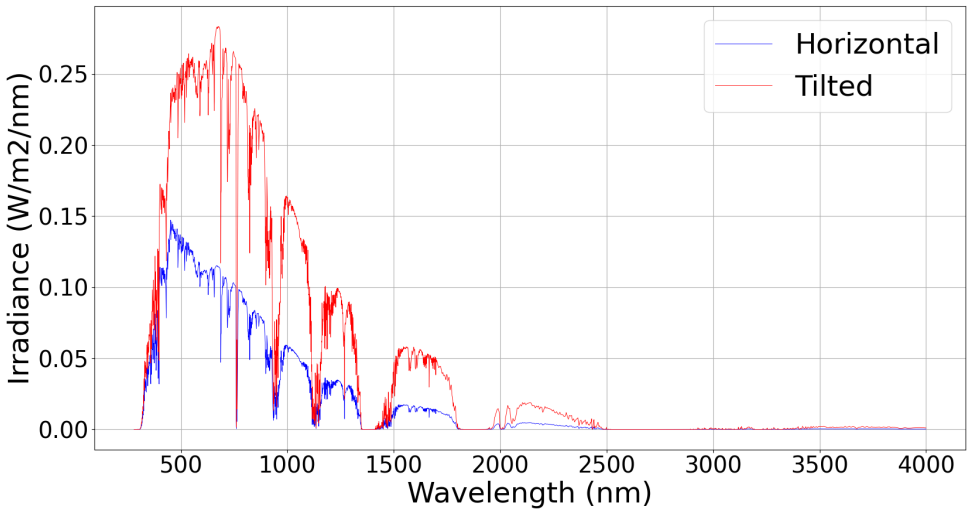

Figure A.19: Average spectral distribution of GHI and GTI, November 2021

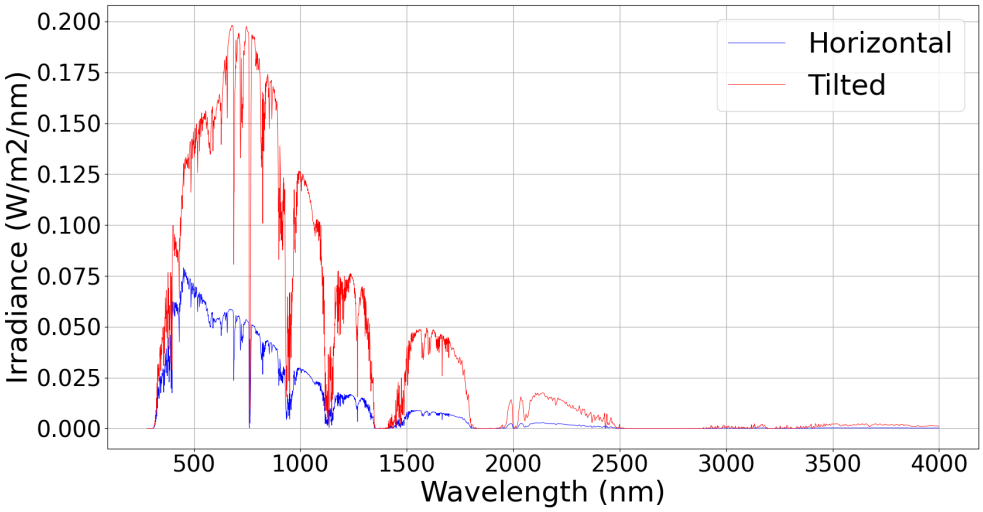

Figure A.20: Average spectral distribution of GHI and GTI, December 2021

Appendix B

Appendix B

Script for finding irradiance, photon flux, APE and watt hours for GHI and GTI for each minute

```
import os
import numpy as np
import pandas as pd
import datetime
from scipy.integrate import simpson
import matplotlib.pyplot as plt
from sklearn.linear_model import LinearRegression

q = 1.60217663e-19 #Elementary electron charge (Coulombs)
h = 6.62607015e-34 #Planck's constant (m2.kg/s)
c = 299792458. #speed of light (m/s)

#NOTE: this is the folder that contains the folders of all months (it ...
    should be referred to 2020)
path_main_folder = r'D:\2020data'

month = 'December' #NOTE: change the month to get another month

path_folder = path_main_folder + '\\' + month  #NOTE: all folders should ...
    have only the name of the month


days_list = os.listdir(path_folder) #gets a list of all days folders


file_results = 'results_' + month + '.csv'


data_all=pd.DataFrame(columns=['TimeStamp','I_GH','fi_GH','APE_GH', 'Wh_GH',

                               'I_GT','fi_GT','APE_GT', 'Wh_GT'])



for day in days_list: #loops for each day folder

    print('DAY: ', day)

    minutes_list = os.listdir(path_folder + '\\' + day) #gets a list with ...
        all minute files

    for minute in minutes_list: #loops for each minute file
```

```
        print('file: ', minute)

        timestamp = minute[:-4]

        dataset = pd.read_csv(path_folder + '\\' + day + '\\' + minute, ...
            skiprows=range(1, 21), nrows=900) #reads the minute file, a-Si ...
            53 - 475, CIGS 23 - 941, CdTe 22 - 549



        #calculations with Global Horizontal spectral irradiance

        intensity_GH = np.array(dataset['Global horizontal spectral ...
            irradiance from 280-4000nm (W/m2/nm)']) #intensity Gobal ...
            Horizontal spectral irradiance (W/m2/nm)

        wavelength = np.linspace(300,1200,len(intensity_GH)) #wavelength (nm)

        photon_flux_GH = intensity_GH/(h*c/wavelength)*10**-9 #photon flux ...
            Global Horizontal spectral irradiance (#photons/(m2.s))

        I_GH = simpson(intensity_GH) #(W/m2)

        fi_GH = simpson(photon_flux_GH) #(#photons/(m2.s)).nm

        APE_GH = 1/q*(I_GH/fi_GH) #eV

        Wh_GH = I_GH*(1/60) #Wh/m2



        #calculations with Global Tilted spectral irradiance
        I_GT = np.nan

        fi_GT = np.nan

        APE_GT = np.nan

        Wh_GT = np.nan

        if 'Global tilted spectral irradiance from 280-4000nm (W/m2/nm)' ...
            in dataset.columns:
            intensity_GT = np.array(dataset['Global tilted spectral ...
                irradiance from 280-4000nm (W/m2/nm)'])

            photon_flux_GT = intensity_GT/(h*c/wavelength)*10**-9

            I_GT = simpson(intensity_GT) #(W/m2)

            fi_GT = simpson(photon_flux_GT) #(#photons/(m2.s)).nm

            APE_GT = 1/q*(I_GT/fi_GT) #eV

            Wh_GT = I_GT*(1/60) #Wh


        data_dict = {'TimeStamp': [timestamp], 'I_GH': [I_GH], 'fi_GH': ...
            [fi_GH], 'APE_GH': [APE_GH], 'Wh_GH': [Wh_GH],

                     'I_GT': [I_GT], 'fi_GT': [fi_GT], 'APE_GT': [APE_GT], ...
                        'Wh_GT': [Wh_GT]}
```

```
        data_all=pd.concat([data_all, pd.DataFrame.from_dict(data_dict)], ...
            ignore_index=True)


data_all['TimeStamp'] = ...
    pd.to_datetime(data_all['TimeStamp'],format='%Y-%m-%d_%H-%M')#_uAdger_Site_Spectral_

data_all.to_csv(path_main_folder + '\\' + file_results, index=False)

Tot_Wh_GH = data_all['Wh_GH'].sum() #Wh/m2
Tot_Wh_GT = data_all['Wh_GT'].sum() #Wh/m2

data_all['I_GH'].mean()

APE_GH_average = data_all['APE_GH'].mean()
APE_GT_average = data_all['APE_GT'].mean()

print(APE_GH_average, APE_GT_average)


#%%

#plotting spectral distribution
y_H = dataset['Global horizontal spectral irradiance from 280-4000nm ...
    (W/m2/nm)']
y_T = dataset['Global tilted spectral irradiance from 280-4000nm (W/m2/nm)']


f1 = plt.figure()
plt.plot(wavelength, y_H, linewidth =.6, color = 'blue', label= 'Horizontal')
plt.plot(wavelength, y_T, linewidth =.6, color = 'red', label= 'Tilted')
#plt.title('March 2020 Horizontal vs Tilted', fontsize=19)
plt.ylabel('Irradiance (W/m2/nm)', fontsize=35)
plt.xlabel('Wavelength (nm)', fontsize=35)
plt.legend(loc='best', fontsize = 35)
plt.xticks(fontsize=28)
plt.yticks(fontsize=28)
plt.grid()
plt.show()

y_GH = data_all['I_GH'].values
y_GT = data_all['I_GT'].values

f2 = plt.figure()
plt.plot(data_all['TimeStamp'], y_GH, linewidth =.6, color = 'blue', ...
    label= 'Horizontal')
plt.plot(data_all['TimeStamp'], y_GT, linewidth =.6, color = 'red', label= ...
    'Tilted')
plt.title('', fontsize=19)
plt.ylabel('Irradiance (W/m2)', fontsize=17)
plt.xlabel('Time', fontsize=17)
plt.legend(loc='best', fontsize = 17)
plt.xticks(fontsize=14)
plt.yticks(fontsize=14)
plt.grid()
plt.show()
```

Appendix C

Appendix C

Script for finding average values for each month

```
import os
import numpy as np
import pandas as pd
import datetime
from scipy.integrate import simpson
import matplotlib.pyplot as plt
import math

q = 1.60217663e-19 #Elementary electron charge (Coulombs)
h = 6.62607015e-34 #Planck's constant (m2.kg/s)
c = 299792458. #speed of light (m/s)
#A = 0.02743
#a = -3.65
#b = -0.075
#Temp_delta = 3
#E_0 = 1000

hours_GH = 5.394 #irradiance based on wavelength range solar cell picks ...
    up, changes on month######
hours_GT = 14.425 #irradiance based on wavelength range solar cell picks ...
    up, changes on month######
Temp_air = 0.4 #average air temp for month, changes depending on month######
#Ws = 2.06 #average wind speed for month, changes depending on month######

NOCT = 45 #C, changes depending on type of solar cell
P_Temp_coeff = 0.33 # %/C, changes depending on type of solar cell
Voc = 69.5 #STC, changes based on type of solar panel
FF = 0.72 #STC, changes based on type of solar panel

dataEQE = pd.read_excel(r'D:\EQE_CdTe.xlsx', sheet_name = 0) #Containing ...
    list of EQE values for each wavelength, change depending on PV module
df = pd.DataFrame(dataEQE)
df['EQE_CdTe'] = df['EQE_CdTe'] / 100

#NOTE: this is the folder that contains the folders of all months (it ...
    should be referred to 2020)
path_main_folder = r'D:\2021data'
month = 'December' #NOTE: change the month to get another month
path_folder = path_main_folder + '\\' + month  #NOTE: all folders should ...
    have only the name of the month
days_list = os.listdir(path_folder) #gets a list of all days folders
file_results = 'results_' + month + '.csv'
```

```
wavelength = np.arange(280,4001,1) #wavelength (nm)
sum_intensity_GH = np.zeros(len(wavelength))
sum_intensity_GT = np.zeros(len(wavelength))
num_minutes_GH = 0
num_minutes_GT = 0

#for day in days_list: #loops for each day folder

for day in days_list:

    print('DAY: ', day)

    minutes_list = os.listdir(path_folder + '\\' + day) #gets a list with ...
       all minute files

#    for minute in minutes_list: #loops for each minute file

    for minute in minutes_list: #loops for each minute file

        print('file: ', minute)

        dataset = pd.read_csv(path_folder + '\\' + day + '\\' + minute) ...
           #reads the minute file


        #calculations with Global Horizontal spectral irradiance

        num_minutes_GH += 1

        sum_intensity_GH += np.array(dataset[dataset.columns[0]]) ...
           #intensity Gobal Horizontal spectral irradiance (W/m2/nm)


        #calculations with Global Tilted spectral irradiance

        if len(dataset.columns) >= 2:

            num_minutes_GT += 1

            sum_intensity_GT += np.array(dataset[dataset.columns[1]]) ...
               #intensity Gobal Tilted spectral irradiance



avg_intensity_GH = sum_intensity_GH/num_minutes_GH
avg_intensity_GT = sum_intensity_GT/num_minutes_GT

I_GH_tot = simpson(avg_intensity_GH) #(W/m2)
I_GT_tot= simpson(avg_intensity_GT) #(W/m2)

avg_PF_GH = avg_intensity_GH/(h*c/wavelength)*10**-9
avg_PF_GT = avg_intensity_GT/(h*c/wavelength)*10**-9

results_data = pd.DataFrame({'wavelength': wavelength[(wavelength>=301) & ...
   (wavelength<=849)],
                             'Avg_GH': avg_intensity_GH[(wavelength>=301) ...
                                & (wavelength<=849)],
                             'Avg_GT': avg_intensity_GT[(wavelength>=301) ...
                                & (wavelength<=849)],
                             'Avg_PF_GH': avg_PF_GH[(wavelength>=301) & ...
                                (wavelength<=849)],
```

```
                                'Avg_PF_GT': avg_PF_GT[(wavelength>=301) & ...
                                    (wavelength<=849)]}) #Creates a data ...
                                    frame that picks out values form a given ...
                                    wavelenth range

N_electron_GH = results_data['Avg_PF_GH']*dataEQE['EQE_CdTe']
Isc_lambda_GH = N_electron_GH * q
Tot_Isc_GH = Isc_lambda_GH.sum() # A/m2

N_electron_GT = results_data['Avg_PF_GT']*dataEQE['EQE_CdTe']
Isc_lambda_GT = N_electron_GT * q
Tot_Isc_GT = Isc_lambda_GT.sum() # A/m2

Temp_cell_GH = Temp_air + ((NOCT-20)/800) * I_GH_tot # degrees celsius
Temp_cell_GT = Temp_air + ((NOCT-20)/800) * I_GT_tot# degrees celsius

P_mod_GH = Tot_Isc_GH * Voc * FF # W/m2
P_mod_GT = Tot_Isc_GT * Voc * FF # W/m2

P_mod_GH_real = P_mod_GH - P_mod_GH*(P_Temp_coeff/100)*(25-Temp_cell_GH) #W
P_mod_GT_real = P_mod_GT - P_mod_GT*(P_Temp_coeff/100)*(25-Temp_cell_GT) #W

E_mod_GH = P_mod_GH_real * hours_GH #Wh per month
E_mod_GT = P_mod_GT_real * hours_GT #Wh per month

#%%
#Plots the average spectral distribution graph for the given month
f1 = plt.figure()
plt.plot(wavelength, avg_intensity_GH, linewidth =.6, color = 'blue', ...
    label= 'Horizontal')
#plt.plot(wavelength[(wavelength>=300) & (wavelength<=1500)],
#         avg_intensity_GH[(wavelength>=300) & (wavelength<=1500)], ...
    linewidth =.6, color = 'blue', label= 'Horizontal')
plt.plot(wavelength, avg_intensity_GT, linewidth =.6, color = 'red', ...
    label= 'Tilted')
#plt.title('March 2020 Horizontal vs Tilted', fontsize=19)
#plt.title('Average irradiance February 2020')
plt.ylabel('Irradiance (W/m2/nm)', fontsize=35)
plt.xlabel('Wavelength (nm)', fontsize=35)
plt.legend(loc='best', fontsize = 35)
plt.xticks(fontsize=28)
plt.yticks(fontsize=28)
plt.grid()
plt.show()
```

Appendix D

Appendix D

The python script for Figure 4.9, 4.11, 4.10 and 4.12

```
import pandas as pd
import matplotlib.pyplot as plt

# Define the months
months = ['Jan', 'Feb', 'Mar', 'Apr', 'May', 'Jun', 'Jul', 'Aug', 'Sep', ...
    'Oct', 'Nov', 'Dec']

# The data is given in this order
order = ['Jan', 'Feb', 'Mar', 'Apr','May', 'Jun', 'Jul', 'Sep', 'Oct', ...
    'Nov', 'Dec']

# Define the data
kWh_2021_c_Si = [83.088, 52.710, 462.467, 828.497, 383.151, 488.066, ...
    722.723, 311.090, 164.598, 59.264, 32.584] # changeing values ...
    depending on year and incident angle
kWh_2021_a_Si = [27.408, 20.090, 188.074, 352.102, 171.575, 221.691, ...
    322.906, 136.352, 66.657, 21.701, 9.823]
kWh_2021_CdTe = [53.402, 36.714, 332.841, 612.703, 294.793, 379.921, ...
    558.644, 236.320, 118.986, 40.633, 20.053]
kWh_2021_CIGS = [125.294, 78.061, 669.727, 1187.612, 545.403, 688.950, ...
    1018.189, 444.012, 239.250, 87.675, 49.220]

# Create DataFrame
df_2020_1 = pd.DataFrame(list(zip(order, kWh_2021_c_Si)), columns = ...
    ['Month', 'Wh'])
df_2020_2 = pd.DataFrame(list(zip(order, kWh_2021_a_Si)), columns = ...
    ['Month', 'Wh'])
df_2020_3 = pd.DataFrame(list(zip(order, kWh_2021_CdTe)), columns = ...
    ['Month', 'Wh'])
df_2020_4 = pd.DataFrame(list(zip(order, kWh_2021_CIGS)), columns = ...
    ['Month', 'Wh'])

# Set Month as index for easier manipulation
df_2020_1.set_index('Month', inplace=True)
df_2020_2.set_index('Month', inplace=True)
df_2020_3.set_index('Month', inplace=True)
df_2020_4.set_index('Month', inplace=True)

# Reindex to include all months
df_2020_1 = df_2020_1.reindex(months)
df_2020_2 = df_2020_2.reindex(months)
df_2020_3 = df_2020_3.reindex(months)
df_2020_4 = df_2020_4.reindex(months)
```

```
# Figure size
plt.figure(figsize=(10, 6))

# Plot the data for consecutive months
plt.plot(df_2020_1.index[1:5], df_2020_1['Wh'][1:5], marker='o', ...
    label='c-Si', color = 'blue')
plt.plot(df_2020_1.index[4:], df_2020_1['Wh'][4:], marker='o', color = 'blue')

plt.plot(df_2020_2.index[1:5], df_2020_2['Wh'][1:5], marker='o', ...
    label='a-Si', color = 'black')
plt.plot(df_2020_2.index[4:], df_2020_2['Wh'][4:], marker='o', color = ...
    'black')

plt.plot(df_2020_3.index[1:5], df_2020_3['Wh'][1:5], marker='o', ...
    label='CdTe', color = 'green')
plt.plot(df_2020_3.index[4:], df_2020_3['Wh'][4:], marker='o', color = ...
    'green')

plt.plot(df_2020_4.index[1:5], df_2020_4['Wh'][1:5], marker='o', ...
    label='CIGS', color = 'red')
plt.plot(df_2020_4.index[4:], df_2020_4['Wh'][4:], marker='o', color = 'red')

plt.xlabel('Month', fontsize=35)
plt.ylabel('kWh/m2', fontsize=35)
plt.legend(fontsize=35)
plt.xticks(fontsize=28)
plt.yticks(fontsize=28)
plt.grid()
plt.show()
```

Bibliography

[1] *Introduction to Solar Radiation*. [Online]. Available: https://www.newport.com/t/introduction-to-solar-radiation (Accessed: 20- 5-2023).

[2] *Average Solar Radiation | PVEducation*. [Online]. Available: https://www.pveducation.org/pvcdrom/properties-of-sunlight/average-solar-radiation (Accessed: 21- 5-2023).

[3] *Solar radiation modeling | Solargis*. [Online]. Available: https://solargis.com/docs/methodology/solar-radiation-modeling (Accessed: 1- 5-2023).

[4] *Solar Irradiance Concepts: DNI, DHI, GHI & GTI - Yellow Haze Solar Power*. [Online]. Available: https://www.yellowhaze.in/solar-irradiance/ (Accessed: 10- 5-2023).

[5] *Electromagnetic Spectrum*. [Online]. Available: https://imagine.gsfc.nasa.gov/science/toolbox/emspectrum2.html (Accessed: 1- 3-2023).

[6] *Spectral Irradiance | PVEducation*. [Online]. Available: https://www.pveducation.org/pvcdrom/properties-of-sunlight/spectral-irradiance (Accessed: 8- 4-2023).

[7] *Air Mass | PVEducation*. [Online]. Available: https://www.pveducation.org/pvcdrom/properties-of-sunlight/air-mass (Accessed: 6- 3-2023).

[8] *Introduction to Solar Simulators*. [Online]. Available: https://www.azom.com/article.aspx?ArticleID=10817 (Accessed: 1- 3-2023).

[9] *Standard Test Conditions (STC) of a Photovoltaic Panel*. [Online]. Available: https://www.alternative-energy-tutorials.com/photovoltaics/standard-test-conditions.html (Accessed: 31- 3-2023).

[10] *How do solar panels work? | Live Science*. [Online]. Available: https://www.livescience.com/41995-how-do-solar-panels-work.html (Accessed: 9- 5-2023).

[11] *Solar PV Modules*. [Online]. Available: https://www.solardirect.com/archives/pv/pvlist/pvlist.htm (Accessed: 11- 4-2023).

[12] *Solar Panel Construction — Clean Energy Reviews*. [Online]. Available: https://www.cleanenergyreviews.info/blog/solar-panel-components-construction (Accessed: 20- 5-2023).

[13] *Types of Solar Panels: Which One Is the Best Choice?* [Online]. Available: https://www.solarreviews.com/blog/pros-and-cons-of-monocrystalline-vs-polycrystalline-solar-panels (Accessed: 12- 4-2023).

[14] *Crystalline Silicon Photovoltaics Research | Department of Energy*. [Online]. Available: https://www.energy.gov/eere/solar/crystalline-silicon-photovoltaics-research (Accessed: 20- 5-2023).

[15] *Amorphous Silicon Solar Cells: structure and applications*. [Online]. Available: https://sinovoltaics.com/learning-center/solar-cells/amorphous-silicon-solar-cells-structure-and-applications/ (Accessed: 1- 5-2023).

[16] *How Do Thin Film Solar Panels Work?* [Online]. Available: https://www.solarreviews.com/blog/thin-film-solar-panels (Accessed: 2- 5-2023).

[17] *Cadmium Telluride | Department of Energy*. [Online]. Available: https://www.energy.gov/eere/solar/cadmium-telluride (Accessed: 1- 5-2023).

[18] *Cadmium Telluride Solar Cells | Photovoltaic Research | NREL*. [Online]. Available: https://www.nrel.gov/pv/cadmium-telluride-solar-cells.html (Accessed: 13- 4-2023).

[19] *Copper Indium Gallium Diselenide Solar Cells | Photovoltaic Research | NREL*. [Online]. Available: https://www.nrel.gov/pv/copper-indium-gallium-diselenide-solar-cells.html (Accessed: 1- 5-2023).

[20] G. Nofuentes, C. A. Gueymard, J. Aguilera, M. D. Pérez-Godoy, and F. Charte, "Is the average photon energy a unique characteristic of the spectral distribution of global irradiance?" *Solar Energy*, vol. 149, pp. 32–43, Jun. 2017, ISSN: 0038-092X. DOI: 10.1016/J.SOLENER.2017.03.086.

[21] *Solar Spectral and Module Temperature Influence on the Outdoor Performance of Thin Film PV Modules Deployed on a Sunny Inland Site*. [Online]. Available: https://www.hindawi.com/journals/ijp/2013/620127/ (Accessed: 17- 5-2023).

[22] *Solar Spectral Irradiance under Clear and Cloudy Skies: Measurements and a Semiempirical Model in: Journal of Applied Meteorology and Climatology Volume 30 Issue 4 (1991)*. [Online]. Available: https://journals.ametsoc.org/view/journals/apme/30/4/1520-0450_1991_030_0447_ssiuca_2_0_co_2.xml (Accessed: 17- 5-2023).

[23] *What is the Difference Between Internal and External Quantum Efficiency | Compare the Difference Between Similar Terms*. [Online]. Available: https://www.differencebetween.com/what-is-the-difference-between-internal-and-external-quantum-efficiency/ (Accessed: 11- 5-2023).

[24] *Quantum Efficiency | PVEducation*. [Online]. Available: https://www.pveducation.org/pvcdrom/solar-cell-operation/quantum-efficiency (Accessed: 29- 4-2023).

[25] *Open-Circuit Voltage | PVEducation*. [Online]. Available: https://www.pveducation.org/pvcdrom/solar-cell-operation/open-circuit-voltage (Accessed: 8- 5-2023).

[26] *Short-Circuit Current | PVEducation*. [Online]. Available: https://www.pveducation.org/pvcdrom/solar-cell-operation/short-circuit-current (Accessed: 8- 5-2023).

[27] *Fill Factor | PVEducation*. [Online]. Available: https://www.pveducation.org/pvcdrom/solar-cell-operation/fill-factor (Accessed: 9- 5-2023).

[28] *Solar Cell Efficiency | PVEducation*. [Online]. Available: https://www.pveducation.org/pvcdrom/solar-cell-operation/solar-cell-efficiency (Accessed: 10- 5-2023).

[29] *Effect of Temperature | PVEducation*. [Online]. Available: https://www.pveducation.org/pvcdrom/solar-cell-operation/effect-of-temperature (Accessed: 29- 4-2023).

[30] *Nominal Operating Cell Temperature | PVEducation*. [Online]. Available: https://www.pveducation.org/pvcdrom/modules-and-arrays/nominal-operating-cell-temperature (Accessed: 11- 4-2023).

[31] J. A. Kratochvil, W. E. Boyson, and D. L. King, "Photovoltaic array performance model.," *Sandia Report No. 2004-3535*, vol. 8, pp. 1–19, Aug. 2004. DOI: 10.2172/919131. [Online]. Available: http://www.osti.gov/bridge/product.biblio.jsp?osti_id=919131.

[32] *Shunt Resistance | PVEducation*. [Online]. Available: https://www.pveducation.org/pvcdrom/solar-cell-operation/shunt-resistance (Accessed: 11- 5-2023).

[33] *Series Resistance | PVEducation*. [Online]. Available: https://www.pveducation.org/pvcdrom/solar-cell-operation/series-resistance (Accessed: 11- 5-2023).

[34] *Impact of Both Series and Shunt Resistance | PVEducation*. [Online]. Available: https://www.pveducation.org/pvcdrom/solar-cell-operation/impact-of-both-series-and-shunt-resistance (Accessed: 11- 5-2023).

[35] E. E. Looney, Z. Liu, A. Classen, *et al.*, "Representative identification of spectra and environments (RISE) using k-means," *Progress in Photovoltaics: Research and Applications*, vol. 29, no. 2, pp. 200–211, Feb. 2021, ISSN: 1099159X. DOI: 10.1002/PIP.3358.

[36] W. Jessen, S. Wilbert, C. A. Gueymard, *et al.*, "Proposal and evaluation of subordinate standard solar irradiance spectra for applications in solar energy systems," *Solar Energy*, vol. 168, pp. 30–43, Jul. 2018, ISSN: 0038-092X. DOI: 10.1016/J.SOLENER.2018.03.043.

[37] T. Minemoto, Y. Nakada, H. Takahashi, and H. Takakura, "Uniqueness verification of solar spectrum index of average photon energy for evaluating outdoor performance of photovoltaic modules," *Solar Energy*, vol. 83, no. 8, pp. 1294–1299, Aug. 2009, ISSN: 0038-092X. DOI: 10.1016/J.SOLENER.2009.03.004.

[38] S. Yoshida, S. Ueno, N. Kataoka, H. Takakura, and T. Minemoto, "Estimation of global tilted irradiance and output energy using meteorological data and performance of photovoltaic modules," *Solar Energy*, vol. 93, pp. 90–99, Jul. 2013, ISSN: 0038-092X. DOI: 10.1016/J.SOLENER.2013.04.001.

[39] *IBC Solar | MonoSol 305/310 GX5 | Solar Panel Datasheet | ENF Panel Directory*. [Online]. Available: https://www.enfsolar.com/pv/panel-datasheet/crystalline/35862 (Accessed: 6- 5-2023).

[40] *Kaneka | U-EA Type 100-120W | Solar Panel Datasheet | ENF Panel Directory*. [Online]. Available: https://www.enfsolar.com/pv/panel-datasheet/Thin-film/647?utm_source=ENF&utm_medium=panel_list&utm_campaign=enquiry_product_directory&utm_content=2448 (Accessed: 9- 5-2023).

[41] "TS-Suite100 WS High Performance Low-Voltage Photovoltaic Modules," [Online]. Available: www.toledosolar-inc.com (Accessed: 6- 5-2023).

[42] *Eterbright Solar | CIGS-3000A1 Series | Solar Panel Datasheet | ENF Panel Directory*. [Online]. Available: https://www.enfsolar.com/pv/panel-datasheet/Thin-film/935 (Accessed: 12- 5-2023).

[43] *WebPlotDigitizer - Extract data from plots, images, and maps*. [Online]. Available: https://automeris.io/WebPlotDigitizer/index.html.

[44] "MAXEON™ GEN III SOLAR CELLS Durability Advantage," 2017. [Online]. Available: http://us.sunpower.com/about/sunpower-technology/patents/ (Accessed: 29- 4-2023).

[45] B. Minnaert and P. Veelaert, "A proposal for typical artificial light sources for the characterization of indoor photovoltaic applications," *Energies*, vol. 7, no. 3, pp. 1500–1516, 2014, ISSN: 19961073. DOI: 10.3390/EN7031500.

[46] H. Dang and V. P. Singh, "Nanowire CdS-CdTe Solar Cells with Molybdenum Oxide as Contact," *Scientific Reports*, vol. 5, Oct. 2015, ISSN: 20452322. DOI: 10.1038/SREP14859.

[47] *(PDF) Development of four-terminal devices utilising thin-film solar cells*. [Online]. Available: https://www.researchgate.net/publication/333974132_Development_of_four-terminal_devices_utilising_thin-film_solar_cells.

[48] *SolarSIM-G | Spectrafy*. [Online]. Available: https://www.spectrafy.com/products/solarsim-g (Accessed: 15- 5-2023).

[49] Asadollah Bagheri, "Work Report Solar Spectral Measurement at UIA (PV Lab.), Characterization of HR2000+, unpublished," UiA, Tech. Rep., 2017.

[50] Adrian Bjørge Ulven, "Comparing a portable spectrometer with a stationary broadband Spectrafy instrument based on spectral irradiance distribution and APE," Ph.D. dissertation, UiA, Grimstad, 2022, pp. 4–5.